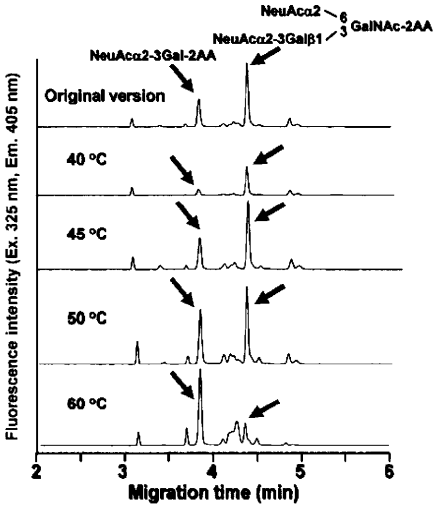

Figure 3. Optimization for oligosaccharide releasing reaction. O-Glycans released from the model glycopeptide by the automatic glycan-releasing system were analyzed by CE after labeling with 2-AA. The most upper panel shows the results on the analysis of O-glycans in the model glycopeptide using the original version of the auto glycan releasing system. The similar results were observed at 45 °C. Analytical conditions for CE: capillary, DB-1 capillary (100 m i.d., 30 cm); running buffer, 100 mM Tris-borate buffer (pH 8.3) containing 5% PEG70000; applied voltage, 25 kV; injection, pressure method (1 psi for 5 s); temperature, 25 °C; detection, helium–cadmium laser-induced fluorescence (excitation 325 nm, emission 405 nm).

exchange resin and a reactor having 136 μL volume. In addition, the dead volume was minimized by removing the detector. The volume (15 μL) of the sample solution was also fixed. In this device (Figure 1), the sample solution is brought to the reactor, then the flow is stopped for a specified time, and the releasing reaction occurs in the reactor. Then, the flow brings the sample zone to the cartridge (50 μL volume). It should be noted that these modifications minimizes diffusion of the sample zone, and the reaction mixture was recovered with the minimal dilution.

We optimized the conditions for glycan releasing reaction using a model glycopeptide derived from caseinoglycomacropeptide (cow milk) having the sequence GEPTSTPT.[17] Disialyl-T antigen, (NeuAcα2–3Galβ1-3(NeuAcα2-6)GalNAc, attaches to the fourth Thr residue (shown in bold face with underline) from the N-terminal. NeuAcα2-3Galβ1-3-residue of the disialyl T antigen is labile under alkaline conditions and forms degradation product (NeuAcα2-3Gal) by β-elimination (i.e., peeling reaction).[17,18] After the releasing reaction, the mixture of the released oligosaccharides was labeled with 2AA and analyzed by CE (Figure 3).

The disialyl-T and the degradation product (NeuAcα2-3Gal-2AA) were observed at 4.4 and 3.8 min, respectively. The best yield of disialyl-T was observed at 45 °C. At 40 °C, the yield of disialyl-T was lower than that at 45 °C. At the higher temperatures than 50 °C, the abundance of the peeling product (i.e., NeuAcα2-3Galβ1-3) became higher. The yield of the disialyl T from the model peptide obtained under the optimized conditions (reaction solution, 0.5 M LiOH; reaction time, 3 min; reaction temperature, 45 °C) was 58.8 ± 3% (n = 5) when determined by CE. The ratio of the degradation product was 24.4 ± 1%. It should be noted that the present method showed excellent repeatability, although partial degradation was observed.

Hyphenation of AGC with a Spotter Machine for MALDI MS Measurement. We directly connected the auto glycan releasing system to the spotter machine for MALDI MS measurement (Figure 2). The effluent from the cartridge was divided by a splitter, and a 10% portion of the effluent was introduced to the MALDI spotter. By adjusting the length and the internal diameter of tubing (0.15 mm i.d., 60 cm length), we could introduce one tenth of the sample solution to the MALDI plate and the effluent was automatically mixed with an aqueous solution of the matrix (DHB). However, we could not detect the molecular ions due to free O-glycans released from the core peptides with high sensitivity (data not shown). This is probably due to the presence of contaminated peptide fragments and other materials during the releasing reaction.

To improve the sensitivity in detection of the glycans, on-plate derivatization of O-glycans in the effluent collected on the MALDI plate was examined. Lattova et al. reported that phenylhydrazine was a useful derivatization reagent for highly sensitive detection of glycans in clinical samples. The method is based on on-plate derivatization of glycans with phenylhydrazine to form phenylhydrazone. The phenylhydrazone thus formed on the plate was detected by a MALDI-MS apparatus.[23,24] In the present study, we introduced a 1.25% aqueous solution of phenylhydrazine to be mixed with the effluent from AGC, and the mixture was spotted onto the plate, on which DHB solution had been previously spotted and dried. The mixture on the target was kept at 37 °C for 1 h to complete the derivatization reaction according to the method reported by Lattova et al.[23,24] We can use a diluted phenylhydrazine solution due to its high reaction efficiency in hydrazone formation. In addition, because the effluent was passed through a cartridge packed with cation exchange resin, it showed acidic property which is preferable for hydrazone formation. It should be noticed that phenylhydrazone derivatives of reducing carbohydrates are easily crystallizable and may be a strong point for MALDI MS measurement. In addition, it was not necessary to

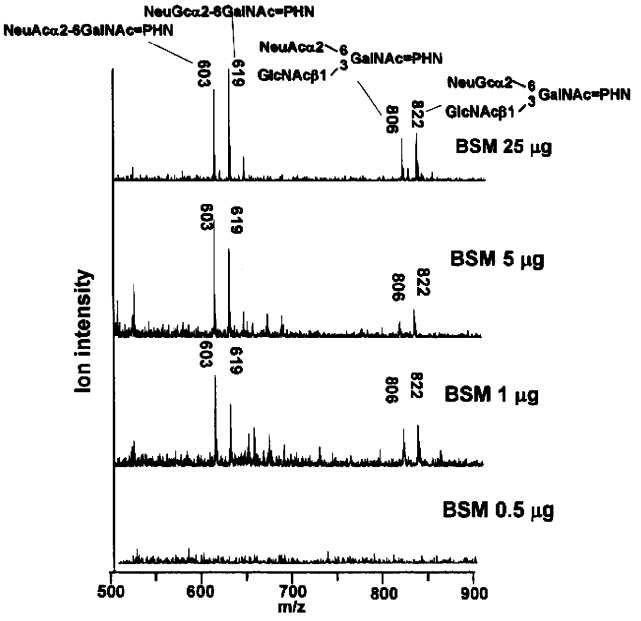

Figure 4. Detection limit of the autoglycan releasing system-MS system as examined using bovine submaxillary mucin as a model sample.

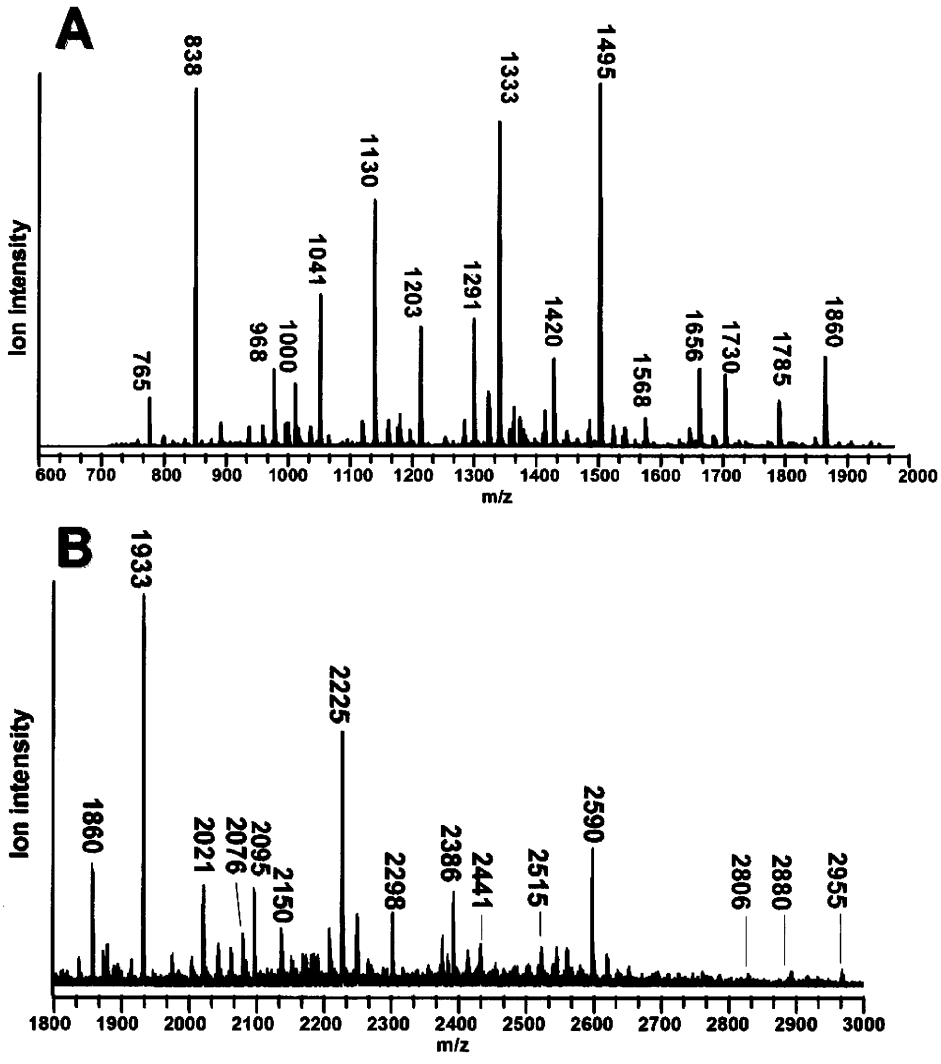

Figure 5. Analysis of O-glycans from MKN45 cells. The results for the low- and high-mass ranges are shown in parts A and B, respectively.

remove the excess phenylhydrazine by washing. Thus, the whole procedure from the releasing of O-glycans to MS measurement was completed within 1.5 h.

On the basis of the studies described above, we applied the present technique to the analysis of O-glycans from bovine submaxillary mucin (BSM). The results are shown in Figure 4.

When using 25 μg of BSM (2.5 μg as the injected amount), we could easily observe the major molecular ions due to O-glycans. Two molecular ions observed at m/z 603 and m/z 619 are due to NeuAcα2-6GalNAc=PHN and NeuGcα2-6GalNAc=PHN, respectively. Two molecular ions observed at m/z 806 and 822 are confirmed as sialyl-core 3 structures, GlcNAcβ1-3(NeuAcα2−6) GalNAc=PHN and GlcNAcβ1-3(NeuGcα2-6) GalNAc=PHN, respectively. Sialic acids of O-glycans in BSM have two forms of *N*-acetyl neuraminic acid and *N*-glycolyl neuraminic acid. Therefore, we could observe two sets of the molecular ions of O-glycans.[11] Even at the 1 μg-level of the sample (0.1 μg as the amount injected to the MALDI plate), we clearly observed the molecular ions of these glycans.

(23) Lattova, E.; Chen, V. C.; Varma, S.; Bezabeh, T.; Perreault, H. *Rapid Commun. Mass Spectrom.* **2007**, *21*, 1644–1650.

(24) Lattova, E.; Kapkova, P.; Krokhin, O.; Perreault, H. *Anal. Chem.* **2006**, *78*, 2977–2984.

Application to the Analysis of O-Glycans Derived from Cancer Cells. We applied the present method to the analysis of O-glycans expressed on MKN45 cells (a human stomach cancer cell line). O-Glycans of glycopeptide fractions obtained from the whole cells after digestion with Pronase were analyzed by the present method. The results observed for low- and high-molecular ranges are shown in parts A and B of Figure 5, respectively, and the list of the proposed structures based on our previously reported data is summarized in Table 1.[18]

Two molecular ion peaks observed at m/z 838 and m/z 1041 are due to asialo core 2 type structures, Galβ1-3(Galβ1-4GlcNAcβ1-6)-GalNAc=PHN and Galβ 1-3(GlcNAcβ- Galβ1-4GlcNAcβ1-6)-GalNAc=PHN, respectively. Four molecular ion peaks at m/z 1203, 1568, 1933, and 2298 are confirmed as asialo polylactosamine-type O-glycans, Galβ1-3((Galβ-GlcNAcβ)$_n$-Galβ1-4-GlcNAcβ1-6) GalNAc=PHN (n = 1−4). The molecular ion peak observed at m/z 765 corresponds to sialyl-T, NeuAcα2-3Galβ1-3GalNAc=PHN. Three molecular ion peaks observed at m/z 968, 1130, and 1333 are assigned as monosialo core 2 type glycans, Galβ1-3(GlcNAcβ1-6)GalNAc=PHN + NeuAc$_1$, Galβ1-3(Galβ1-4GlcNAcβ1-6) GalNAc=PHN + NeuAc$_1$, and Galβ1-3(GlcNAcβ-Galβ1-4GlcNAcβ1-6)GalNAc=PHN + NeuAc$_1$, re-

Table 1. O-Glycans Observed in MKN45 Cells

proposed structures	observed molecular mass (*m/z*)
Asialo Glycans	
Galβ1-3(Galβ1-4GlcNAcβ1-6)GalNAc=PHN	838
Galβ1-3(GlcNAc-Galβ1-4GlcNAcβ1-6)GalNAc=PHN	1041
Galβ1-3(Gal-GlcNAc-Galβ1-4GlcNAcβ1-6)GalNAc=PHN	1203
Galβ1-3((Gal-GlcNAc)$_2$-Galβ1-4GlcNAcβ1-6)GalNAc=PHN	1568
Galβ1-3((Gal-GlcNAc)$_3$-Galβ1-4GlcNAcβ1-6)GalNAc=PHN	1933
Galβ1-3((Gal-GlcNAc)$_4$-Galβ1-4GlcNAcβ1-6)GalNAc=PHN	2298
Monosilao Glycans	
NeuAcα2-3Galβ1-3GalNAc=PHN	765
Galβ1-3(GlcNAcβ1-6)GalNAc=PHN + NeuAc$_1$	968
Galβ1-3(Galβ1-4GlcNAcβ1-6)GalNAc=PHN + NeuAc$_1$	1130
Galβ1-3(GlcNAc-Galβ1-4GlcNAcβ1-6)GalNAc=PHN + NeuAc$_1$	1333
Galβ1-3(Gal-GlcNAc-Galβ1-4GlcNAcβ1-6)GalNAc=PHN + NeuAc$_1$	1495
Galβ1-3((Gal-GlcNAc)$_2$-Galβ1-4GlcNAcβ1-6)GalNAc=PHN + NeuAc$_1$	1860
Galβ1-3((Gal-GlcNAc)$_3$-Galβ1-4GlcNAcβ1-6)GalNAc=PHN + NeuAc	2225
Galβ1-3((Gal-GlcNAc)$_4$-Galβ1-4GlcNAcβ1-6)GalNAc=PHN + NeuAc	2590
Galβ1-3((Gal-GlcNAc)$_5$-Galβ1-4GlcNAcβ1-6)GalNAc=PHN + NeuAc	2955
Disialo Glycans	
NeuAc-Galβ1-3(NeuAc-Galβ1-4GlcNAcβ1-6)GalNAc=PHN	1420
NeuAc-Galβ1-3(NeuAc-Gal-GlcNAc-Galβ1-4GlcNAcβ1-6)GalNAc=PHN	1785
NeuAc-Galβ1-3(NeuAc-(Gal-GlcNAc)$_2$-Galβ1-4GlcNAcβ1-6)GalNAc=PHN	2150
NeuAc-Galβ1-3(NeuAc-(Gal-GlcNAc)$_3$-Galβ1-4GlcNAcβ1-6)GalNAc=PHN	2515
NeuAc-Galβ1-3(NeuAc-(Gal-GlcNAc)$_4$-Galβ1-4GlcNAcβ1-6)GalNAc=PHN	2880
Trisialo Glycans	
NeuAc-Gal-GlcNAc-(NeuAc-Gal-GlcNAc)Galβ1-3(NeuAcα2-6)GalNAc=PHN	2076
NeuAc-Gal-GlcNAc-(NeuAc-Gal-GlcNAc)Galβ1-3(NeuAcα2-6)GalNAc=PHN + Gal-GlcNAc	2441
NeuAc-Gal-GlcNAc-(NeuAc-Gal-GlcNAc)Galβ1-3(NeuAcα2-6)GalNAc=PHN + (Gal-GlcNAc)$_2$	2806
Degradation Product	
(Gal-GlcNAc)$_2$-Gal=PHN	1000
NeuAc-(Gal-GlcNAc)$_2$-Gal=PHN	1291
NeuAc-(Gal-GlcNAc)$_3$-Gal=PHN	1656
(Gal-GlcNAc)$_4$-Gal=PHN	1730
NeuAc-(Gal-GlcNAc)$_4$-Gal=PHN	2021
(Gal-GlcNAc)$_5$-Gal=PHN	2095
NeuAc-(Gal-GlcNAc)$_5$-Gal=PHN	2386

spectively. Five molecular ion peaks at *m/z* 1495, 1860, 2225, 2590, and 2955 are due to monosialo polylactosamine-type O-glycans, Galβ1-3((Galβ-GlcNAcβ)$_n$-Galβ1-4GlcNAcβ1-6)GalNAc=PHN + NeuAc$_1$ ($n = 1-5$). Disialo polylactosamine-type O-glycans were also observed in MKN45 cells. Four molecular ion peaks at *m/z* 1785, 2150, 2515, and 2880 are confirmed as disialo core 2 type glycans modified with 1−7 units of lactosamine residues. Three molecular ion peaks containing three sialic acid residues were observed at *m/z* 2076, 2441, and 2806 are due to $NeuAc_3Hex_3HexNAc_3$=PNH, $NeuAc_3Hex_4HexNAc_4$=PNH, and $NeuAc_3Hex_5HexNAc_5$=PNH, respectively. As reported previously, these trisialo glycans are core 1 type glycans having the structures as indicated below.[18]

NeuAcα(Galβ1-4GlcNAcβ)nNeuAcα2-6GalNAc
NeuAcα(Galβ1-4GlcNAcβ)mGalβ1-3

These structures were observed exclusively in MKN45 cells according to our recent research results, and we suggested that these O-glycans might be a specific marker of gastric adenocarcinoma.[18] Seven molecular ion peaks observed at *m/z* 1000, 1291, 1656, 1730, 2021, 2095, and 2386 are due to the degradation products from these trisialo core 1 type polylactosamine glycans, NeuAc-(Galβ-GlcNAcβ)$_n$-Gal=PHN ($n = 1-5$), and the presence of these products means that these glycans occupy the 1-3 linked arm of the glycans because of easy degradation (i.e., peeling). Therefore, these glycans are important keys for structural confirmation of the parent glycans.[18]

Analysis of O-Glycans Derived from Serum Glycoproteins Using AGC-MS System. Another application to the analysis of O-glycans in a serum sample is shown in Figure 6. After brief deionization of the diluted solution using an ultramembrane filter, the solution was easily analyzed by the present system. As indicated in Figure 6A, several molecular ions were observed. The molecular ion peaks observed at *m/z* 765 with sodium adduct ion (*m/z* 787) are confirmed as sialyl-T.

The molecular ion peak observed at *m/z* 1056 corresponds to disialyl-T. The molecular ion peaks observed at *m/z* 562 with sodium adduct ion *m/z* 584 are due to a peeling product (NeuAc α2-3Gal=PNH). After the releasing reaction is performed in the flow of an aqueous LiOH solution, the reaction mixture is passed through a cartridge packed with cation exchange resin. Therefore, the effluent from the device does not contain cation(s) as examined by the absence of Li adduct ion in the MS spectra. Then, the effluent from the device is mixed with diluted phenylhydrazine solution and spotted onto the MALDI plate. Accordingly, the phenylhydrazone on the MALDI plate theoretically only shows protonated ions. In this case, however, diluted phenylhydrazine solution probably contains a trace amount of sodium ion, and the MS gives sodium adduct ions as well as protonated ions.

To confirm these peaks, we also analyzed the O-glycans obtained from the split effluent (collected by the fraction collector)

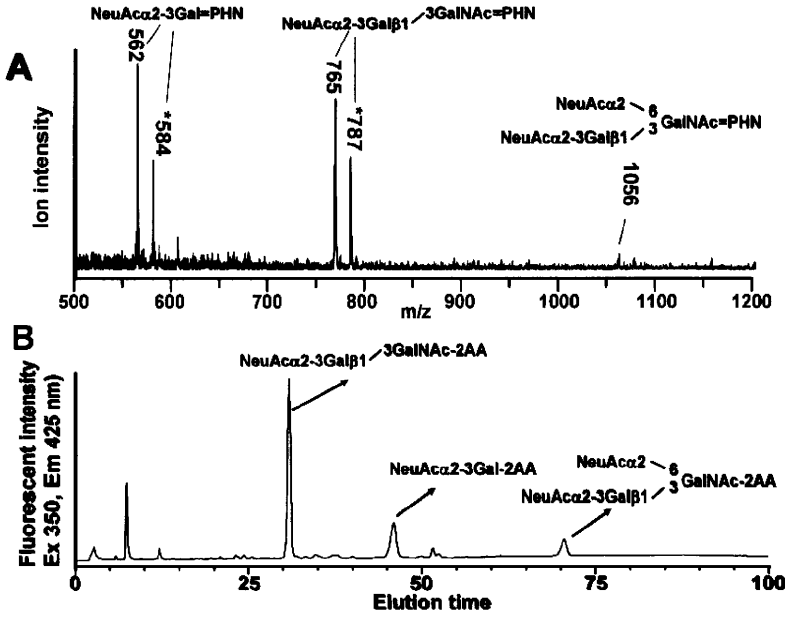

Figure 6. Analysis of O-glycans in a pooled serum sample. (A) MS analysis of the O-glycans by the present method. (B) Analysis of the O-glycans in a pooled serum sample by HPLC. The nine tenth portions of the O-glycans released by the autoglycan releasing system-MS system were labeled with 2-AA and analyzed by HPLC. Analytical conditions for HPLC: column, Asahi Shodex NH2P-50 4E (4.6 mm × 250 mm); eluent, solvent A, 2% CH_3COOH in acetonitrile; solvent B, 5% CH_3COOH/3% triethylamine in water, gradient condition, linear gradient (30−95% solvent B) from 2 to 82 min, maintained for 20 min.

as 2-AA derivatives using HPLC (Figure 6B). Each of the peaks was collected and compared with the standard samples by MALDI-TOF MS as reported previously.[18] The most abundant peak observed at 31 min is due to sialyl-T which shows the molecular ion at m/z 765. The peak observed at 71 min is derived from disialyl-T which shows the molecular ion at m/z 1085. We also observed the peak due to the peeling product (NeuAcα2-3Gal-2AA) at 45 min. These results were in good agreement with the direct MS analysis as shown in Figure 6A, although the relative abundances of these glycans are different between HPLC and MS methods. The HPLC/CE-fluorescent detection method affords accurate amounts of the glycans based on the fluorescent intensity of the 2-aminobenzoic acid residue at the reducing terminal. A combination of both methods will be a powerful tool for accurate diagnosis of the disease or disease states.

CONCLUSIONS

We have been developing an automatic device for releasing O-glycans from the mucin-type glycoproteins.[17−19] In the present paper, we connected the device to a spotter machine for MALDI MS measurement and attempted direct measurement of O-glycans. Because we could not observe the molecular ions of free glycans by direct measurement due to their low sensitivity and the presence of contaminated materials during releasing reactions, we labeled the released O-glycans with phenylhydrazine by *in situ* derivatization to achieve highly sensitive detection of O-glycans by MS measurement. The derivatization reaction proceeded under mild conditions even in the presence of 2,5-dihydroxybenzoic acid (matrix material). Accordingly, we performed the analysis from the glycan releasing reaction to MS measurement within 1.5 h.

The system allows MS analysis of O-glycans of bovine submaxillary mucin even when using 1 μg of the protein sample (actual sample amount 100 ng). We applied the present technique to the analysis of the O-glycans expressed on MKN45 cells derived from human stomach adenocarcinoma and found that trisialo-O-glycans were present abundantly as reported previously.[18] In addition, O-glycans in a pooled serum sample were also successfully analyzed. It is well-known that quantitative analysis is often difficult in MS measurement. Fluorescence detection by HPLC/CE gives robust and reproducible results in quantitative analysis. The data in Figure 6 indicate that the proposed method using the hyphenated glycan-releasing and MS analysis shows similar glycan profiles with those obtained by HPLC, but the relative abundances of the glycans are somewhat different from those observed by HPLC/CE analysis. However, extremely high-throughput characteristics of the present method will be quite important in routine analysis of glycans for clinical use. We believe that the present technique is the primary attempt to use MS measurement for routine clinical diagnostic works.

Received for review June 15, 2010. Accepted July 20, 2010.

AC101581N

Research Article

Biomedical Chromatography

Received 16 April 2010, Revised 3 June 2010, Accepted 4 June 2010 Published online in Wiley InterScience

(www.interscience.wiley.com) DOI 10.1002/bmc.1486

Determination of sulfate ester content in sulfated oligo- and poly-saccharides by capillary electrophoresis with indirect UV detection

Mitsuhiro Kinoshita[a], Naotaka Kakoi[a], Yu-ki Matsuno[b], Takao Hayakawa[c] and Kazuaki Kakehi[a]*

ABSTRACT: Carbohydrates having sulfate groups such as glycosaminoglycans and chemically synthesized sucrose sulfate show interesting and important biological activities. We adapted CE with indirect UV detection technique to the determination of sulfate ester in sulfated carbohydrates, which were previously hydrolyzed with HCl. The liberated sulfate ion was analyzed using a background electrolyte consisting of triethanolamine-buffered chromate with hexamethonium bromide. Sulfate contents of glucose 3-sulfate and sucrose octasulfate used as a model were in good agreement with theoretical values (accuracy, 95.9–96.7 and 97.4–101.9%, respectively), and relative standard deviation values run-to-run were 0.977 and 1.90%, respectively. We applied the method to the determination of the sulfate contents of some glycosaminoglycan samples and showed that the contents were in good agreement with those calculated from sulfur content. Copyright © 2010 John Wiley & Sons, Ltd.

Keywords: sulfate; glycosaminoglycans; capillary electrophoresis indirect UV detection

Introduction

Sulfation of hydroxyl and amino groups (-O-SO_3H and -NH-SO_3H) is one of the common modifications of carbohydrates and is often observed in various glycoconjugates such as proteoglycans or mucin-like glycoproteins. Sulfated carbohydrates are widely distributed in animals as the major constituents of proteoglycans and are biologically active molecules involved in various biological events (Hooper *et al.*, 1996; Honke and Taniguchi, 2002; Wu, 2006). Functions of sulfated carbohydrates strongly depend on the presence and spatial positioning in the molecules. Degree of sulfation on carbohydrates is also closely related to biological activities such as blood coagulation, signal transduction and cell–cell interaction (Lindahl *et al.*, 1983; Villanueva, 1984; Hemmerich and Rosen, 1994; Small *et al.*, 1996; Tsuboi *et al.*, 1996). Chemical sulfation of carbohydrates often affords compounds showing novel biological activities such as anti-HIV activities (Katsuraya *et al.*, 1994, 1999; Yoshida *et al.*, 1995; Hattori *et al.*, 1998). Sulfated carbohydrates also have potential as pharmaceuticals (Werz and Seeberger, 2005). Sucrose octasulfate, 'Sucralfate' and the chemically synthesized octasulfated pentasaccharide 'Arixtra' are used as antiulcer and anticoagulant drugs, respectively (Candelli *et al.*, 2000; Giangrande, 2002).

In view of these interesting features of sulfated carbohydrates, assessment of sulfate content is important not only for the understanding of their biological significance but also the development and manufacturing of novel bioactive sulfated carbohydrates. Several methods have been developed for the determination of sulfate content of carbohydrates. Classical methods are based on the colorimetric determination of the inorganic sulfate ion liberated from sulfated carbohydrates by acid hydrolysis, such as chelating barium ions with rhodizonate (Terho and Hartiala, 1971; Roy and Turner, 1982). Srinivasan *et al.* achieved the determination of microgram quantity of sulfate ion based on the formation of stable complex of sulfate ester with *n*-butylamine and achieved determination of microgram quantity of sulfate ion (Srinivasan *et al.*, 1970). Unfortunately, these methods are not suitable for the determination of a small amount of sulfate ester in complex carbohydrate, because they are time-consuming and not sensitive enough, require a significant amount of material, and are prone to interference from the other ions. Compared with these conventional methods, ion chromatography (IC) demonstrates increased specificity and sensitivity

* Correspondence to: K. Kakehi, Faculty of Pharmaceutical Sciences, Kinki University, Kowakae 3-4-1, Higashi-osaka 577-8502, Japan. E-mail: k_kakehi@phar.kindai.ac.jp

[a] Faculty of Pharmaceutical Sciences, Kinki University, Kowakae 3-4-1, Higashi-osaka 577-8502, Japan

[b] Research Center for Medical Glycoscience, National Institute of Advanced Industrial Science and Technology, Open Space Laboratory C-2, 1-1-1 Umezono, Tsukuba, Ibaraki 305-8568, Japan

[c] Pharmaceutical Research and Technology Institute, Kinki University, Kowakae 3-4-1, Higashi-osaka 577-8502, Japan

Abbreviations used: BGE, background electrolyte; CSA, chondroitin sulfate A; DMF, *N*,*N*-dimethylformamide; DS, dermatan sulfate; GAG, glycosaminoglycan; HA, hyaluronic acid; HMB, hexamethonium bromide; HP, heparin; HS, heparan sulfate; TBA, tributylamine; TEA, triethanolamine.

as well as the inherent ability for the determination of various inorganic ions, and has been applied to the analysis of the ions in the samples from biological, environmental and industrial origins (Lopez-Ruiz, 2000). The sulfate contents in glycoproteins or GAGs were successfully determined by IC (Cole and Evrovski, 1997; Toida *et al.*, 1999). Toida *et al.* liberated the sulfate ion from chemically O-sulfated GAGs by acid hydrolysis, and determined it by a combination of IC and conductivity detection (Tadano-Aritomi *et al.*, 2001).

Capillary electrophoresis (CE) is a powerful tool for separation of inorganic ions with high resolving power. Its performance is comparable with that of IC, and has become one of the standard tools for the analysis of inorganic ions in environmental, biomedical, clinical and industrial samples (Fritz, 2000; Timerbaev, 2002, 2004; Johns *et al.*, 2003; Pacakova *et al.*, 2003; Paull and King, 2003). CE allows rapid analysis with high resolution and exhibits good capabilities in quantitative analysis, making it well suited for routine analysis of sulfate content of carbohydrates. Although the detection in CE is usually performed by direct UV detection, most inorganic ions lack a chromophore and cannot be detected using common direct UV detection. Therefore, indirect UV detection technique is usually used for determination of inorganic ions. Indirect UV detection adds an UV-absorbing co-ion (called the probe) to the background electrolyte (BGE) and this probe is displaced by migration, causing a negative signal. Indirect UV detection is an effective alternative detection technique for inorganic ions. The attractive performance of the CE method has been employed for the assay of sulfotransferase activity (Saillard *et al.*, 1999). Thus, CE is considered a useful alternative to the well-established IC method for routine analysis of sulfate content of carbohydrates.

In the present study, we developed a method using capillary electrophoresis with indirect UV detection to the determination of sulfate content of sulfated oligo-/polysaccharides, and applied the method for the determination of sulfate content in some sulfated GAGs and the monitoring of chemically sulfation reaction of polysaccharides. The present method will provide a robust method for the analysis of sulfated carbohydrates using routinely available laboratory instrumentation.

Experimental

Materials

Hexamethonium bromide, glucose 3-sulfate (sodium salt, 98% purity by HPLC), sucrose octasulfate (sodium salt) and heparin from bovine intestinal mucosa were purchased from Sigma (St Louis, MO, USA). Hyaluronic acid (from *Streptococcus zooepidemicus*) was purchased from Nacalai tesque (Uji, Kyoto, Japan). Chondroitin sulfate A (from whale cartilage), dermatan sulfate (from pig skin) and heparan sulfate (from bovine kidney) were purchased from Seikagaku Biobusiness (Chiyoda-ku, Tokyo, Japan). Tributylamine (TBA), *N,N*-dimethylformamide (DMF) and pyridine–sulfur trioxide complex were obtained from Wako Pure Chemicals (Dosho-machi, Osaka, Japan). All other chemicals and reagents were of the highest grade or HPLC grade. Running buffers and aqueous solutions were prepared with water purified with a Milli-Q purification system (Millipore, Bedford, MS, USA).

Sulfation of Chondroitin Sulfate A

Chemical sulfation of chondroitin sulfate A was performed according to the method reported by Maruyama *et al.* (1998). The sodium salt (10 mg) of chondroitin sulfate A (from whale cartilage) was dissolved in 1 mL of 5% TBA–HCl water (pH 2.8), and then the solution was lyophilized to dryness to give the tributylammonium salt. The salt was dissolved in 1 mL of DMF, and pyridine–sulfur trioxide complex (10, 50, 100 and 250 mg) was added. After incubating the mixture for 1 h at 40°C, the reaction was terminated by addition of water (1 mL). The reaction product was precipitated with cold ethanol (6 mL) saturated with anhydrous sodium acetate, collected by centrifugation at 4°C, then dissolved in water followed by dialysis against water to remove salts and lyophilized. We obtained $PSCS_{10}$ (11.8 mg), $PSCS_{50}$ (14.1 mg), $PSCS_{100}$ (17.2 mg) and $PSCS_{250}$ (18.6 mg), respectively, by changing the amount of pyridine–sulfur trioxide complex.

Sample and Standard Solutions

Standard solutions of sulfate ion were prepared by dissolving an accurately weighed amount of sodium sulfate (300 mg) in water (10 mL; 210 mM). A series of standard solutions of sulfate ion for calibration curve were prepared by appropriate dilution of the standard solution with water. Sample solution of sulfated oligo-/polysaccharides was also prepared by dissolving an accurately weighed amount (1.00 mg) in of water (1 mL).

CE Analysis of Sulfate Ion with Indirect UV Detection

CE was performed with a Beckman P/ACE MDQ system equipped with a UV detector (Beckman Coulter, Fullerton, CA, USA). A fused silica capillary (50 μm i.d., 56 cm effective length, 66 cm total length, from Agilent Technologies) was used throughout the work. The background electrolyte was composed of 10 mM CrO_3–2 mM hexamethonium bromide in 10% MeOH–water (pH 8.0) adjusted with triethanolamine. The background electrolyte was passed through a cellulose acetate membrane filter (0.2 μm). Prior to the first run, the capillary was rinsed with 0.1 M NaOH for 10 min, followed by washing with water for 10 min, and then filled with the background electrolyte. The capillary was conditioned by pre-electrophoresis (−20 kV) for 10 min. After washing the capillary with water and filling with the background electrolyte, samples were automatically injected using pressure injection mode at 1.0 psi for 10 s. Electrophoresis was performed at −20 kV using reverse polarity. Detection was carried out with monitoring the UV absorption at 254 nm. The negative peaks due to the presence of anions in the background of CrO_3 were automatically converted into positive peaks by Beckman 32 Karat software version 4.0 (Beckman Coulter).

Hydrolysis of Sulfated Carbohydrates

A standard solution (20 μL) of glucose 3-sulfate was mixed with 20 μL of 1 M HCl and the mixture was kept at 100°C in a polypropylene tube for specified times. After cooling the mixture to room temperature, the solution (40 μL) was diluted with 1000 μL of water. An aqueous solutions (1000 μL) of $NaNO_3$ was added to the mixture as internal standard and an aliquot (20 μL) was used for the analysis of sulfate ion.

Standard Procedure for the Determination of Sulfate Content in Sulfated Oligo- and Polysaccharides

A solution (20 μL) of sodium salt of sulfated oligo- or polysaccharides was mixed with 20 μL of 1 M HCl, and the mixture was kept at 100°C for 2 h. After cooling the mixture to room temperature, water and the internal standard solutions were added to the mixture as described above and an aliquot was used for the determination of sulfate ion. The content of sulfate ion was calculated from the calibration curve obtained from standard solutions of Na_2SO_4. The percentages of sulfate content were calculated using the following equation:

$$SO_3\,(w/w) = (\text{wt of } SO_4^{2-} \times (\text{wt of } SO_3/\text{wt of } SO_4)/\text{wt of sample}) \times 100$$

where wt (weight) of $SO_3 = 80$, wt of $SO_4^{2-} = 96$, wt of SO_4^{2-} (μg) in hydrolysates is the amount calculated using the calibration curve, and wt of the sample is the amount of the sample in micrograms.

Results and Discussion

Principle

The method is based on the acid hydrolysis of sulfonic acid ester (-O-SO_3H and –NH-SO_3H) followed by the determination of the released sulfate ion (SO_4^{2-}) with CE with indirect UV detection technique. Sulfated oligo-/polysaccharides are hydrolyzed with HCl to produce SO_4^{2-}. In CE, indirect detection is conveniently available for the detection of compounds which do not have chromophores/fluorophores. When non-UV absorbing sulfate ion passes through the UV detector, the zone of SO_4^{2-} causes a negative signal in the background electrolyte containing a UV-absorbing compound as probe. The output polarity of the detection is reversed so that a positive peak is obtained. The content of sulfate ester in parent compounds is calculated using the calibration curve obtained from a standard solution of Na_2SO_4.

Selection of the Background Electrolyte

Selection of the electrolyte (e.g. co-ion and electroosmotic modifier) is important for the sensitive and quantitative determination of sulfate ion. In the present study, chromate ion was selected as the UV absorbing co-ion (probe ion) because of its ionic mobility being close to that of SO_4^{2-}, which ensures high peak symmetry (Johns *et al.*, 2003; Pacakova *et al.*, 2003). We had to pay attention on the presence of high excess amount of chloride ion (Cl^-) in the sample solutions due to the HCl employed for the hydrolysis of sulfate-containing carbohydrates. Inorganic anions by CE are usually analyzed under negative polarity using electroosmotic modifiers such as cationic surfactant, polymer and amines, which improve resolutions of the ions (Haddad *et al.*, 1999; Harakuwe *et al.*, 1999; Kaniansky *et al.*, 1999). Muzikar *et al.* (2003) reported the determination of trace amount of inorganic anions (e.g. SO_4^{2-} or NO_3^-) in the presence of large excess of Cl^- using an electrolyte consisting of triethanolamine (TEA)-buffered chromate with hexamethonium bromide (HMB) as electroosmotic modifier. In the present study, SO_4^{2-} (0.21 mM as Na_2SO_4) was successfully analyzed in the presence of 50 mM HCl using this condition, and Cl^- and SO_4^{2-} were completely resolved and observed at 4.50 and 4.85 min, respectively (Fig. 1a).

We employed nitrate ion (NO_3^-) as internal standard (50 μg/mL, 0.59 mM; Fig. 1b). Ions of SO_4^{2-} and NO_3^- with a huge amount of Cl^- were completely resolved within 5 min. Based on these results, 10 mM CrO_3–2 mM HMB in 10% MeOH–water (pH 8.0 adjusted with TEA) was selected as the background electrolyte throughout the present study.

Linearity and Limit of Detection

The calibration curve for absolute peak area of sulfate ion showed good linearity between 5.0 and 625 μg/mL ($y = 65.4x + 0.58$, $R = 0.9996$; Fig. 2a). In the case of correction of the injection amount by internal standard, the calibration curve exhibited excellent linearity ($y = 0.015x + 0.22$, $R = 0.9999$; Fig. 2b). Both lower limit of detection (LOD) and lower limit of quantification (LOQ) were evaluated on the basis of the standard deviation (σ) and slope (S) from the calibration curve of SO_4^{2-}. In the present conditions, LOD (= 3σ/S) and LOQ (= 10σ/S) were 0.934 and 3.113 μg/mL, respectively.

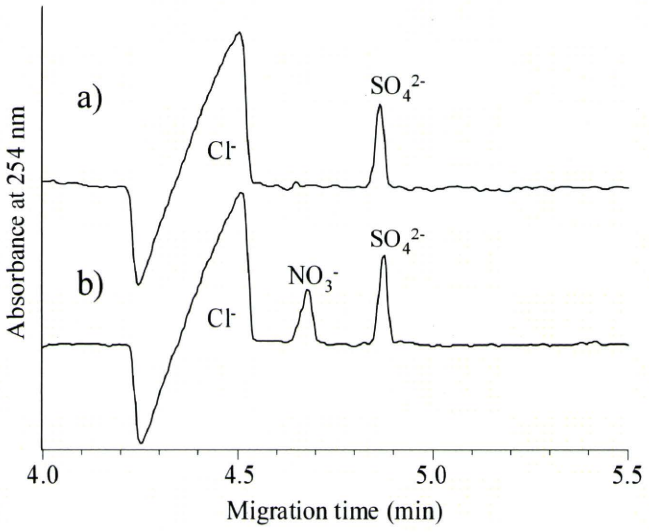

Figure 1. Separation of inorganic anions by CE with indirect UV detection: (a) 0.21 mM sulfate and 50 mM chloride; (b) 0.21 mM sulfate, 50 mM chloride, and 0.59 mM nitrate. Background electrolyte: 10 mM CrO_3/2 mM hexamethonium bromide in 10% MeOH–water at pH 8.0 adjusted with triethanolamine. Capillary: a fused silica capillary (i.d., 50 μm; effective length 56 cm). Applied voltage, –20 kV; temperature, 25°C; sample injection, hydrodynamic injection (1.0 psi, 10 s); detection, indirect UV absorption at 254 nm.

Reproducibility

Run-to-run reproducibility of migration times of SO_4^{2-} and NO_3^- was evaluated using a mixture of 30 μg/mL Na_2SO_4 and 50 μg/mL $NaNO_3$. Migration times of SO_4^{2-} and NO_3^- were 4.96 ± 0.08 and 4.68 ± 0.07, respectively. The relative standard deviation (RSD) was less than 1.4 and 1.6%, respectively ($n = 5$).

Precision

We obtained RSD values in absolute determination of SO_4^{2-} using standard solutions of Na_2SO_4 at 5, 30 and 312.5 μg/mL. The RSD (%) of SO_4^{2-} peak area were 4.58, 2.24 and 2.83%, respectively ($n = 5$; Table 1). In contrast, when using the internal standard (NO_3^-), the RSD (%) of SO_4^{2-} was 1.84, 0.69 and 1.69%, respectively ($n = 5$; Table 1).

Optimization of Conditions for Liberation of SO_4^{2-} by Acid Hydrolysis

Conditions for liberation of SO_4^{2-} from sulfated carbohydrates by acid hydrolysis with HCl were optimized using glucose 3-sulfate as model. After hydrolysis of glucose 3-sulfate with 1 M HCl at 100°C for specified intervals, a portion of the reaction mixture was diluted with water. An aqueous solution of the internal standard ($NaNO_3$) was added, and the released SO_4^{2-} was determined according to the conditions described above.

The content of SO_4^{2-} in the reaction mixture was dependent on hydrolysis time and the hydrolysis was completed within 2 h as shown in Fig. 3(a, b). The excess chloride ion and free glucose produced by hydrolysis in the mixture did not show interference in the determination of SO_4^{2-}. The amount of sulfate ion in glucose 3-sulfate was estimated as 28.1 w/w% (0.96 mol/mol), and showed good agreement with the theoretical values (28.4%). Recoveries were 95.9–96.7% ($n = 5$).

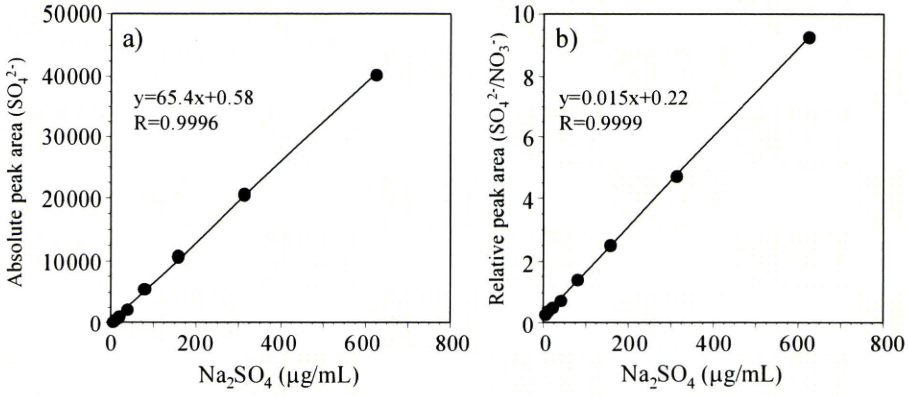

Figure 2. Calibration curve for determination of sulfate ions. (a) Concentration of Na_2SO_4 vs absolute peak area of SO_4^{2-}. (b) Concentration of Na_2SO_4 vs relative peak area (SO_4^{2-}/NO_3^-).

Table 1. Precision results of determination of sulfate ion at three different concentrations

Run	Peak area								
	5 μg/mL Na_2SO_4			30 μg/mL Na_2SO_4			312.5 μg/mL Na_2SO_4		
	SO_4^{2-}	NO_3^-	SO_4^{2-}/NO_3^-	SO_4^{2-}	NO_3^-	SO_4^{2-}/NO_3^-	SO_4^{2-}	NO_3^-	SO_4^{2-}/NO_3^-
1	462	361	1.280	2755	2043	1.349	28041	21505	1.304
2	492	378	1.302	2647	1957	1.353	29945	22869	1.309
3	506	402	1.259	2798	2092	1.337	28762	22214	1.295
4	476	362	1.315	2695	1989	1.355	27945	22290	1.254
5	518	409	1.267	2679	2008	1.334	29013	22452	1.292
Average	491	382	1.284	2715	2018	1.346	28741	22266	1.291
SD	22.5	22.3	0.024	60.8	51.9	0.009	813.6	495.1	0.022
RSD%	4.58	5.83	1.838	2.24	2.57	0.687	2.83	2.22	1.694

We evaluated linearity, repeatability, precision and lower limit of detection using sucrose octasulfate. Sucrose octasulfate is a cytoprotective drug widely used to prevent or treat several gastrointestinal diseases such as gastro-esophageal reflux, gastritis, peptic ulcer, stress ulcer and dyspepsia (Lam and Ching, 1994; Candelli *et al.*, 2000). The sulfate content found in the hydrolysate of sucrose octasulfate showed a good linear relationship with sucrose octasulfate (0.03–1 mg/mL). The value for the relative standard deviation ($n = 5$) of determination of sucrose octasulfate was 1.90% at 250 μg/mL. The limit of detection was 7.8 μg/mL as a solution of sucrose octasulfate sodium salt. When a solution (250 μg/mL) of sucrose octasulfate sodium salt was used, the sulfate content of one batch was 53.1% (accuracy 97.4–101.9%, $n = 5$), which is very close to the theoretical value (54.2%).

Determination of Sulfate Content in Various GAG Samples

Glycosaminoglycans (GAGs) are a family of highly complex and polydisperse linear polysaccharides that display a variety of important biological roles (Jackson *et al.*, 1991; Scott, 1992; Bourin and Lindahl, 1993; Sugahara and Kitagawa, 2000). GAGs are categorized into some main structural groups: hyaluronic acid (HA), chondroitin sulfate A (CSA), dermatan sulfate (DS), heparin (HP) and heparan sulfate (HS) (Zaia, 2009). The structural complexity is compounded by their sequence heterogeneity, primarily caused by variation of the degree and position of sulfate groups. We applied the present method to the determination of sulfate content in some GAG samples. The results are shown in Fig. 4 and Table 2.

Among five GAG samples used in the study, CSA, DS, HP and HS showed sulfate contents of 14.2, 15.0, 25.1 and 11.5%, respectively. HP is mainly composed of trisulfated disaccharide units, α(1-4)-linked L-iduronic acid, which is 2-*O*-sulfated, and D-glucosamine, which is *N*- and 6-*O*-sulfated (Zaia, 2009). Therefore, the sulfate content of HP is higher than those of CSA and DS, which are sulfated at only 4-OH of GalNAc in the disaccharide unit. The sulfate content of HS is lower than those of other sulfated GAGs, because HS from bovine kidney contains unsulfated repeating disaccharide units (GlcAβ1–4GlcNAc) as the major component (~60%), and contains the monosulfated GlcA β1–4GlcNAc (~25%) and the di- or tri-sulfated IdoAα1–4GlcNAc (~15%) (Zaia, 2009). HA, composed of non-sulfated disaccharide units, does not contain sulfate. When hydrolysis step was not included, we did not observe sulfate ions in the electropherograms for all these GAG samples (data not shown). This indicates that inorganic sulfate ion was negligible in the sample. The sulfate contents found in five GAGs were in good agreement with those calculated from sulfur contents provided by the manufacturer (Table 2).

Application to the Monitoring of Chemical Sulfation of Chondroitin Sulfate

Chemical modification of polysaccharides such as sulfation affords novel biological activity, and has been well studied (Srinivasan *et al.*, 1970; Suzuki *et al.*, 2001). We synthesized some preparations of sulfated chondroitin sulfate having different degree of sulfation by changing the amount of pyridine–sulfur

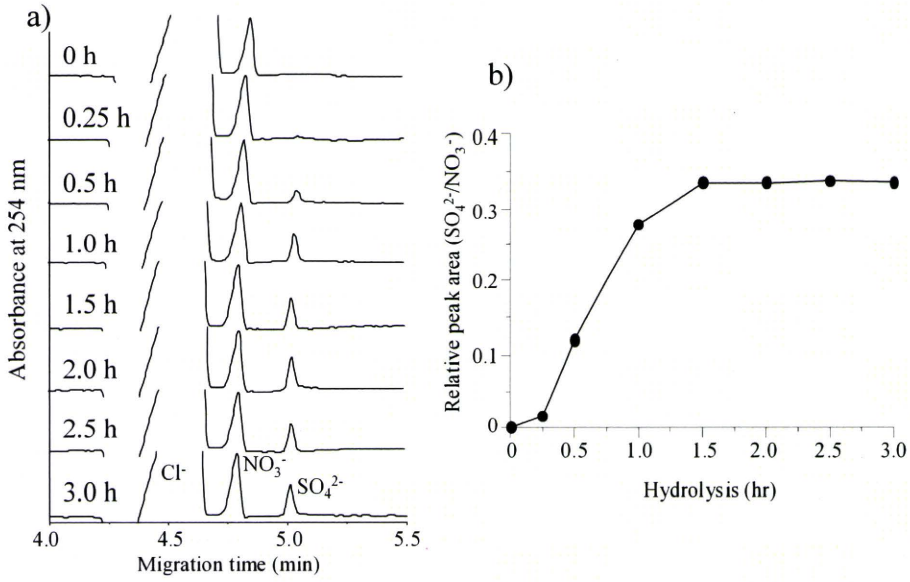

Figure 3. Time course of sulfate liberation during hydrolysis of the glucose 3-sulfate with HCl. (a) Electropherograms of the reaction mixture after hydrolysis. (b) Time course of liberation of sulfate ion from glucose 3-sulfate.

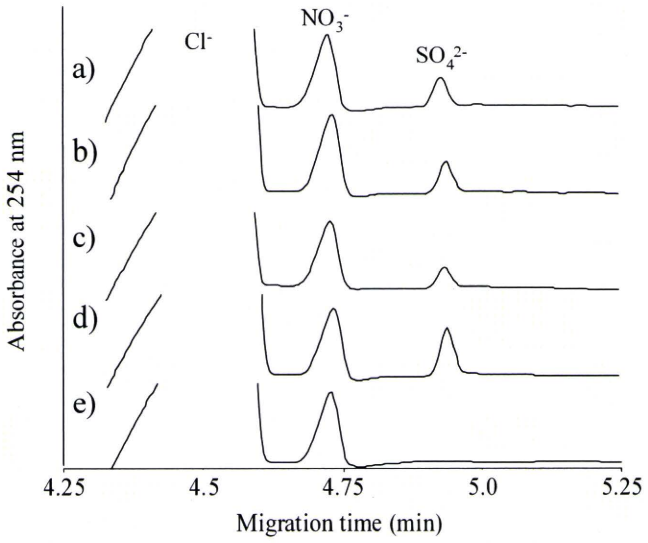

Figure 4. Determination of the sulfate content of some glycosaminoglycans. (a) Chondroitin sulfate A; (b) dermatan sulfate; (c) heparan sulfate; (d) heparin; and (e) hyaluronic acid.

trioxide complex according to the method reported by Maruyama *et al.* (1998). The $PSCS_{10}$, $PSCS_{50}$, $PSCS_{100}$ and $PSCS_{250}$ were obtained from 10 mg CS using 10, 50, 100, and 250 mg pyridine–sulfur complex, respectively. Each preparation was analyzed by the present technique (Table 3).

Sulfate contents calculated from the preparations of $PSCS_{10}$, $PSCS_{50}$, $PSCS_{100}$ and $PSCS_{250}$ were 24.7, 38.5, 45.5 and 48.09%, respectively. The results showed that the amount of pyridine–surfur trioxide complex used in the reaction caused remarkable differences in the sulfate contents, and showed that the present method is useful for monitoring the degree of sulfation during chemical sulfation of oligo-/polysaccharides.

Table 2. Sulfate contents of GAGs

GAGs	Total sulfate (%)[a]	
	Present method	Schoniger method[b]
Hyaluronic acid	n.d.[c]	<0.5
Chondroitin sulfate A	14.2 ± 0.5	15.0
Dermatan sulfate	15.0 ± 0.5	15.5
Heparin	25.1 ± 0.5	25.6
Heparan sulfate	11.5 ± 0.5	11.3

[a] Calculated from the dry weight of GAGs.
[b] Total sulfate contents were calculated from sufur contents provided by manufacturer.
[c] Not detected.

Conclusion

In the present study, we developed a simple, robust and reliable method for the determination of sulfate content in sulfated carbohydrates using CE with indirect UV detection. The background electrolyte consisting of TEA-buffered chromate with HMB is the most appropriate for the analysis of sulfate ion liberated from parent compounds after hydrolysis with HCl.

We applied the present method to the determination of sulfate content in some sulfated GAG samples such as chondroitin sulfate, dermatan sulfate, heparin and heparan sulfate. The sulfate contents found in these GAGs were in good agreement with those obtained by conventional methods. We also applied the method to the determination of sulfate content in chemically sulfated chondroitin sulfate, and revealed the degree of sulfation.

Easy operation of the proposed technique is useful for the determination of sulfate content of sulfated oligo-/polysaccharides. The present method is suitable for routine analysis of sulfate content of carbohydrates.

Table 3. Sulfate contents of chemically sulfated chondroitin sulfate

Sample	Amount of pyridine–sufur trioxide complex	Total sulfate content (%)	Degree of sulfation (%)[b]
CSA[a]	—	14.2	27.5
$PSCS_{10}$	10 mg	24.7	47.6
$PSCS_{50}$	50 mg	38.5	74.6
$PSCS_{100}$	100 mg	45.5	88.2
$PSCS_{250}$	250 mg	48.1	93.2

[a] Chondroitin sulfate A from whale cartilage.
[b] Relative percentage to theoretical value (51.6%) of fully sulfated CSA-30mer.

References

Bourin MC and Lindahl U. Glycosaminoglycans and the regulation of blood coagulation. *Biochemistry Journal* 1993; **289**(Pt 2): 313–330.

Candelli M, Carloni E, Armuzzi A, Cammarota G, Ojetti V, Pignataro G, Santoliquido A, Pola R, Pola E, Gasbarrini G and Gasbarrini A. Role of sucralfate in gastrointestinal diseases. *Panminerva Medicine* 2000; **42**(1): 55–59.

Cole DE, Evrovski J. Quantitation of sulfate and thiosulfate in clinical samples by ion chromatography. *Journal of Chromatography A* 1997; **789**(1–2): 221–232.

Fritz JS. Recent developments in the separation of inorganic and small organic ions by capillary electrophoresis. *Journal of Chromatography A* 2000; **884**(1–2): 261–275.

Giangrande PL. Fondaparinux (Arixtra): a new anticoagulant. *International Journal of Clinical Practice* 2002; **56**(8): 615–617.

Haddad PR, Doble P and Macka M. Developments in sample preparation and separation techniques for the determination of inorganic ions by ion chromatography and capillary electrophoresis. *Journal of Chromatography A* 1999; **856**(1–2): 145–177.

Harakuwe AH, Haddad PR and Davies NW. Effect of drying on the degradation of cationic surfactants and separation performance in capillary zone electrophoresis of inorganic anions. *Journal of Chromatography A* 1999; **863**(1): 81–87.

Hattori K, Yoshida T, Nakashima H, Premanathan M, Aragaki R, Mimura T, Kaneko Y, Yamamoto N and Uryu T. Synthesis of sulfonated aminopolysaccharides having anti-HIV and blood anticoagulant activities. *Carbohydrate Research* 1998; **312**(1–2): 1–8.

Hemmerich S and Rosen SD. 6′-sulfated sialyl Lewis x is a major capping group of GlyCAM-1. *Biochemistry* 1994; **33**(16): 4830–4835.

Honke K and Taniguchi N. Sulfotransferases and sulfated oligosaccharides. *Medical Research Review* 2002; **22**(6): 637–654.

Hooper LV, Manzella SM and Baenziger JU. From legumes to leukocytes: biological roles for sulfated carbohydrates. *FASEB Journal* 1996; **10**(10): 1137–1146.

Jackson RL, Busch SJ and Cardin AD. Glycosaminoglycans: molecular properties, protein interactions, and role in physiological processes. *Physiology Review* 1991; **71**(2): 481–539.

Johns C, Macka M and Haddad PR. Enhancement of detection sensitivity for indirect photometric detection of anions and cations in capillary electrophoresis. *Electrophoresis* 2003; **24**(12–13): 2150–2167.

Kaniansky D, Masar M, Marak J and Bodor R. Capillary electrophoresis of inorganic anions. *Journal of Chromatography A* 1999; **834**(1–2): 133–178.

Katsuraya K, Ikushima N, Takahashi N, Shoji T, Nakashima H, Yamamoto N, Yoshida T and Uryu, T. Synthesis of sulfated alkyl malto- and laminaraoligosaccharides with potent inhibitory effects on AIDS virus infection. *Carbohydrate Research* 1994; **260**(1): 51–61.

Katsuraya K, Nakashima H, Yamamoto N and Uryu T. Synthesis of sulfated oligosaccharide glycosides having high anti-HIV activity and the relationship between activity and chemical structure. *Carbohydrate Research* 1999; **315**(3–4): 234–242.

Lam SK and Ching CK. Sucralfate in clinical practice. *Journal of Gastroenterology and Hepatology* 1994; **9**(4): 401–411.

Lindahl U, Backstrom G and Thunberg L. The antithrombin-binding sequence in heparin. Identification of an essential 6-O-sulfate group. *Journal of Biological Chemistry* 1983; **258**(16): 9826–9830.

Lopez-Ruiz B. Advances in the determination of inorganic anions by ion chromatography. *Journal of Chromatography A* 2000; **881**(1–2): 607–627.

Maruyama T, Toida T, Imanari T, Yu G and Linhardt RJ. Conformational changes and anticoagulant activity of chondroitin sulfate following its O-sulfonation. *Carbohydrate Research* 1998; **306**(1–2): 35–43.

Muzikar M, Havel J and Macka M. Capillary electrophoresis determinations of trace concentrations of inorganic ions in large excess of chloride: soft modelling using artificial neural networks for optimisation of electrolyte composition. *Electrophoresis* 2003; **24**(12–13): 2252–2258.

Pacakova V, Coufal P, Stulik K and Gas B. The importance of capillary electrophoresis, capillary electrochromatography, and ion chromatography in separations of inorganic ions. *Electrophoresis* 2003; **24**(12–13): 1883–1891.

Paull B and King M. Quantitative capillary zone electrophoresis of inorganic anions. *Electrophoresis* 2003; **24**(12–13): 1892–1934.

Roy AB and Turner J. The sulphatase of ox liver. XXIV. The glycosulphatase activity of sulphatase a. *Biochimica Biophysica Acta* 1982; **704**(2): 366–373.

Saillard S, Gareil P, Jozefonvicz J and Daniel R. Development of a capillary electrophoresis assay based on free sulfate determination for the direct monitoring of sulfoesterase activity. *Analytical Biochemistry* 1999; **275**(1): 11–21.

Scott JE. Supramolecular organization of extracellular matrix glycosaminoglycans, *in vitro* and in the tissues. *FASEB Journal* 1992; **6**(9): 2639–2645.

Small DH, Mok SS, Williamson TG and Nurcombe V. Role of proteoglycans in neural development, regeneration, and the aging brain. *Journal of Neurochemistry* 1996; **67**(3): 889–899.

Srinivasan SR, Radhakrishnamurthy B, Dalferes ER Jr and Berenson GS. Determination of sulfate in glycosaminoglycans by gas–liquid chromatography. *Analytical Biochemistry* 1970; **35**(2): 398–404.

Sugahara K and Kitagawa H. Recent advances in the study of the biosynthesis and functions of sulfated glycosaminoglycans. *Current Opinion on Structural Biology* 2000; **10**(5): 518–527.

Suzuki A, Toyoda H, Toida T and Imanari T. Preparation and inhibitory activity on hyaluronidase of fully O-sulfated hyaluro-oligosaccharides. *Glycobiology* 2001; **11**(1): 57–64.

Tadano-Aritomi K, Hikita T, Suzuki A, Toyoda H, Toida T, Imanari T and Ishizuka I. Determination of lipid-bound sulfate by ion chromatography and its application to quantification of sulfolipids from kidneys of various mammalian species. *Journal of Lipid Research* 2001; **42**(10): 1604–1608.

Terho TT and Hartiala K. Method for determination of the sulfate content of glycosaminoglycans. *Analytical Biochemistry* 1971; **41**(2): 471–476.

Timerbaev AR. Recent advances and trends in capillary electrophoresis of inorganic ions. *Electrophoresis* 2002; **23**(22–23): 3884–3906.

Timerbaev AR. Capillary electrophoresis of inorganic ions: an update. *Electrophoresis* 2004; **25**(23–24): 4008–4031.

Toida T, Maruyama T, Suzuki A, Toyoda H, Imanari T and Linhardt RJ. Preparation and anticoagulant activity of fully O-sulphonated glycosaminoglycans. *International Journal of Biology and Macromoles* 1999; **26**(4): 233–241.

Tsuboi S, Isogai Y, Hada N, King JK, Hindsgaul O and Fukuda M. 6`-Sulfo sialyl Lex but not 6-sulfo sialyl Lex expressed on the cell surface supports L-selectin-mediated adhesion. *Journal of Biological Chemistry* 1996; **271**(44): 27213–3716.

Villanueva GB. Predictions of the secondary structure of antithrombin III and the location of the heparin-binding site. *Journal of Biological Chemistry* 1984; **259**(4): 2531–2536.

Werz DB and Seeberger PH. Carbohydrates as the next frontier in pharmaceutical research. *Chemistry* 2005; **11**(11): 3194–3206.

Wu XZ. Sulfated oligosaccharides and tumor: promoter or inhibitor? *Panminerva Medicine* 2006; **48**(1): 27–31.

Yoshida T, Yasuda Y, Mimura T, Kaneko Y, Nakashima H, Yamamoto N and Uryu T. Synthesis of curdlan sulfates having inhibitory effects *in vitro* against AIDS viruses HIV-1 and HIV-2. *Carbohydrate Research* 1995; **276**(2): 425–436.

Zaia J. On-line separations combined with MS for analysis of glycosaminoglycans. *Mass Spectrometry Review* 2009; **28**(2): 254–272.

THE JOURNAL OF BIOLOGICAL CHEMISTRY VOL. 285, NO. 17, pp. 13244–13253, April 23, 2010

Phosphorylation of TRPC6 Channels at Thr^{69} Is Required for Anti-hypertrophic Effects of Phosphodiesterase 5 Inhibition*

Received for publication, October 8, 2009, and in revised form, February 12, 2010 Published, JBC Papers in Press, February 22, 2010, DOI 10.1074/jbc.M109.074104

Motohiro Nishida[‡], Kenta Watanabe[‡], Yoji Sato[§], Michio Nakaya[‡], Naoyuki Kitajima[‡], Tomomi Ide[¶], Ryuji Inoue[‖], and Hitoshi Kurose[‡1]

From the [‡]Department of Pharmacology and Toxicology, Graduate School of Pharmaceutical Sciences, and the [¶]Department of Cardiovascular Medicine, Graduate School of Medical Sciences, Kyushu University, Higashi-ku, Fukuoka 812-8582, the [§]Division of Cellular and Gene Therapy Products, National Institute of Health Sciences, Setagaya, Tokyo 158-8501, and the [‖]Department of Physiology, School of Medicine, Fukuoka University, 7-45-1 Nanakuma, Jyonan-ku, Fukuoka 814-0180, Japan

Activation of Ca^{2+} signaling induced by receptor stimulation and mechanical stress plays a critical role in the development of cardiac hypertrophy. A canonical transient receptor potential protein subfamily member, TRPC6, which is activated by diacylglycerol and mechanical stretch, works as an upstream regulator of the Ca^{2+} signaling pathway. Although activation of protein kinase G (PKG) inhibits TRPC6 channel activity and cardiac hypertrophy, respectively, it is unclear whether PKG suppresses cardiac hypertrophy through inhibition of TRPC6. Here, we show that inhibition of cGMP-selective PDE5 (phosphodiesterase 5) suppresses endothelin-1-, diacylglycerol analog-, and mechanical stretch-induced hypertrophy through inhibition of Ca^{2+} influx in rat neonatal cardiomyocytes. Inhibition of PDE5 suppressed the increase in frequency of Ca^{2+} spikes induced by agonists or mechanical stretch. However, PDE5 inhibition did not suppress the hypertrophic responses induced by high KCl or the activation of protein kinase C, suggesting that PDE5 inhibition suppresses Ca^{2+} influx itself or molecule(s) upstream of Ca^{2+} influx. PKG activated by PDE5 inhibition phosphorylated TRPC6 proteins at Thr^{69} and prevented TRPC6-mediated Ca^{2+} influx. Substitution of Ala for Thr^{69} in TRPC6 abolished the anti-hypertrophic effects of PDE5 inhibition. In addition, chronic PDE5 inhibition by oral sildenafil treatment actually induced TRPC6 phosphorylation in mouse hearts. Knockdown of RGS2 (regulator of G protein signaling 2) and RGS4, both of which are activated by PKG to reduce $G\alpha_q$-mediated signaling, did not affect the suppression of receptor-activated Ca^{2+} influx by PDE5 inhibition. These results suggest that phosphorylation and functional suppression of TRPC6 underlie prevention of pathological hypertrophy by PDE5 inhibition.

Pathological hypertrophy of the heart, induced by pressure overload, such as chronic hypertension and aortic stenosis, is a major risk factor for heart failure and cardiovascular mortality (1). Neurohumoral factors, such as norepinephrine, angiotensin II (Ang II),[2] and endothelin-1 (ET-1), and mechanical stress are believed to be prominent contributors for pressure overload-induced cardiac hypertrophy (2, 3). Neurohumoral factors stimulate G_q protein-coupled receptors, leading to a sustained increase in $[Ca^{2+}]_i$ through activation of phospholipase C. Mechanical stress also increases $[Ca^{2+}]_i$ through Ca^{2+} influx-dependent pathways (4). The increase in $[Ca^{2+}]_i$ induces activation of Ca^{2+}-sensitive effectors, such as Ca^{2+}/calmodulin-dependent serine/threonine phosphatase calcineurin (3, 5), Ca^{2+}/calmodulin-dependent kinase II (6, 7), and calmodulin-binding transcription factor (8), which in turn induces hypertrophic gene expressions. Although the mechanism of Ca^{2+}-mediated hypertrophy is extensively analyzed, it is not fully understood how these Ca^{2+} targets specifically decode the alteration of $[Ca^{2+}]_i$ under the conditions of the rhythmic Ca^{2+} increases required for contraction.

In excitable cardiomyocytes, increases in the frequency or amplitude of Ca^{2+} transients evoked by Ca^{2+} influx-induced Ca^{2+} release have been suggested to encode signals for induction of hypertrophy (9). A partial depolarization of plasma membrane by receptor stimulation is reported to increase the frequency of Ca^{2+} oscillations, leading to activation of nuclear factor of activated T cells (NFAT), a transcription factor that is predominantly regulated by calcineurin (10). Recent reports have indicated that transient receptor potential canonical (TRPC) subfamily proteins play an essential role in agonist-induced membrane depolarization (11, 12). The relevance of TRPC channels to pathological hypertrophy is underscored by the observations that heart-targeted transgenic mice expressing TRPC channels caused hypertrophy (13, 14) and that TRPC proteins were up-regulated in hypertrophied and failing hearts (14–17). Among seven TRPC subfamilies, increased channel activities of TRPC1, TRPC3, and TRPC6 have been implicated in cardiac hypertrophy *in vivo*. TRPC1 is known to function not

* This study was supported by grants from the Ministry of Education, Culture, Sports, Science, and Technology of Japan (to M. Nishida, M. Nakaya, and H. Kurose), a grant-in-aid for scientific research on Innovative Areas (to M. Nishida), a grant-in-aid for scientific research on Priority Areas (H. Kurose), and grants from the Naito Foundation, the Nakatomi Foundation, the Sapporo Bioscience Foundation (M. Nishida), and the Mochida Memorial Foundation for Medical and Pharmaceutical Research (to M. Nakaya).

[1] To whom correspondence should be addressed. Tel./Fax: 81-92-642-6884; E-mail: kurose@phar.kyushu-u.ac.jp.

[2] The abbreviations used are: Ang II, angiotensin II; BNP, brain natriuretic peptide; CA-NFAT, constitutively active NFAT; DAG, diacylglycerol; $DiBAC_4(3)$, bis(1,3-dibutylbarbituric acid)trimethine oxonol; DN-TRPC6, dominant negative TRPC6; ET-1, endothelin-1; BTP2, 4-methyl-4′-[3,5-bis(trifluoromethyl)-1H-pyrazol-1-yl]-1,2,3-thiadiazole-5-carboxanilide; NFAT, nuclear factor of activated T cells; OAG, a DAG derivative, 1-oleoyl-2-acetyl-*sn*-glycerol; TRPC, transient receptor potential canonical; PDE5-I, phosphodiesterase 5-selective inhibitor: 4-{[3′,4′-(methylenedioxy)benzyl]amino}-6-methoxyquinazoline; RGS, regulator of G protein signaling; PKG, protein kinase G; WT, wild type; 8-Br-cGMP, 8-bromo-cyclic GMP; siRNA, small interfering RNA.

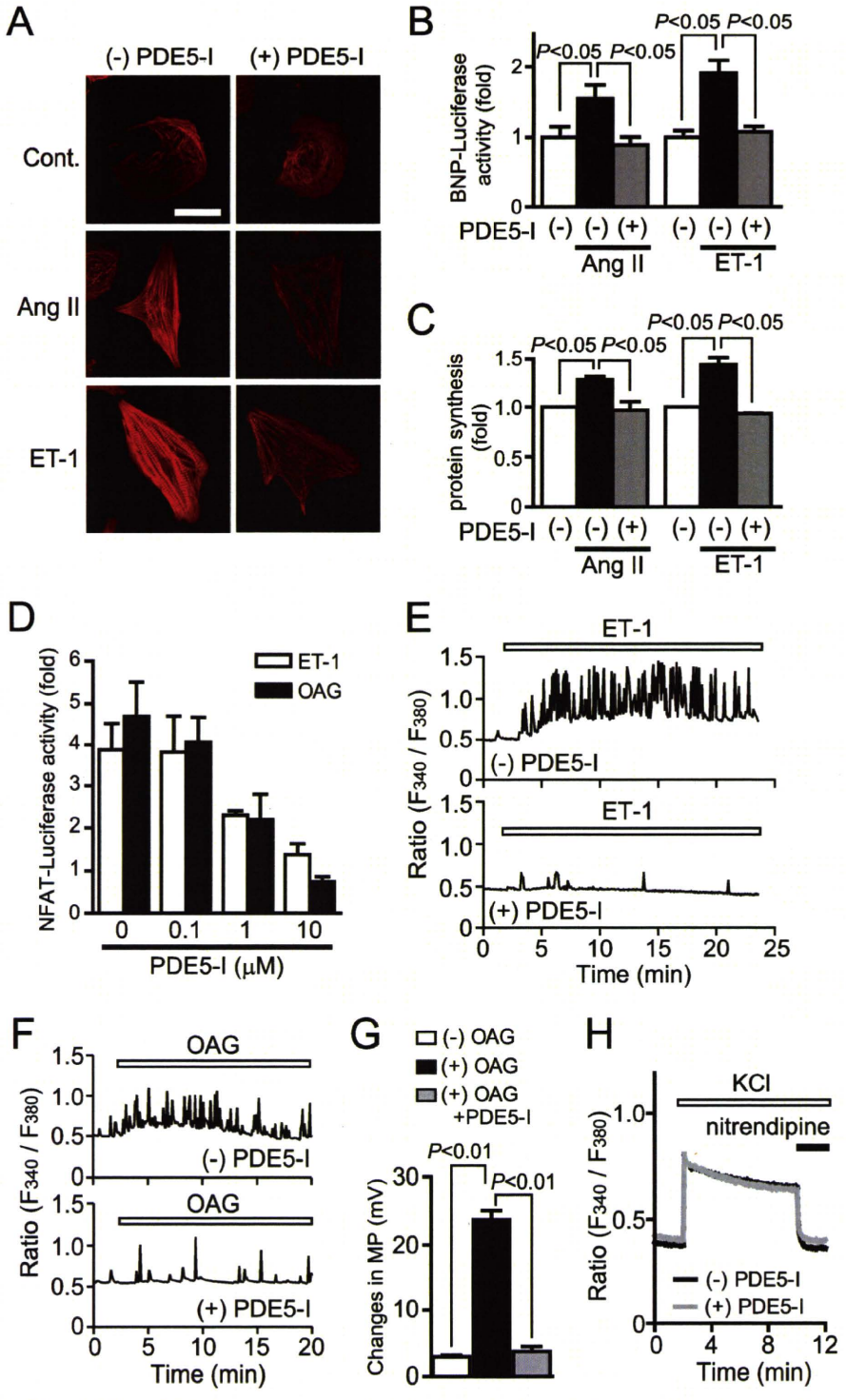

FIGURE 1. **Inhibition of PDE5 suppresses agonist-induced cardiomyocyte hypertrophic responses through inhibition of DAG-mediated Ca^{2+} signaling.** *A–C*, effects of PDE5-I on agonist-induced hypertrophic responses (actin reorganization (*A*), BNP expression (*B*), and protein synthesis (*C*)). Cardiomyocytes were treated with PDE5-I (10 μM) for 20 min before the addition of Ang II (1 μM) or ET-1 (100 nM). *Scale bar*, 50 μm. *D*, effects of PDE5-I on NFAT activation induced by ET-1 and OAG (30 μM). *E–H*, average time courses of Ca^{2+} responses induced by ET-1 (*E*), OAG (*F*), and KCl (*H*) in the absence or presence of PDE5-I. *G*, effects of PDE5-I on OAG-induced increase in membrane potential (*MP*). Cardiomyocytes were treated with OAG for 20 min, and maximal increase in MP was calculated from peak changes in $DiBAC_4(3)$ fluorescence intensity (21). *H*, voltage-dependent Ca^{2+} influx was evoked by KCl (8 mM) for 8 min, and nitrendipine (10 μM) was added to inhibit the activities of voltage-dependent Ca^{2+} channels.

only as a Ca^{2+}-permeable channel-forming subunit but also as an accessory protein to form the Ca^{2+} signaling complex (18). Endogenous TRPC1 and TRPC3 proteins are associated with each other to form native store-operated channels in HEK293 cells (19). In addition, diacylglycerol (DAG)-sensitive TRPC3, TRPC6, and TRPC7 proteins assemble to homotetramers or heterotetramers that function as DAG-activated cation channels (20). We have previously reported that TRPC3 and TRPC6 mediate Ang II-induced membrane depolarization, followed by Ca^{2+} influx through voltage-dependent Ca^{2+} channels in rat neonatal cardiomyocytes (21). Either knockdown of TRPC3 or TRPC6 channels completely suppressed Ang II-induced hypertrophy. Thus, TRPC1, TRPC3, and TRPC6 may form multimers in cardiomyocytes, which function as DAG-activated cation channels. Furthermore, we have recently demonstrated that treatment with a TRPC3 channel-selective blocker suppresses mechanical stretch-induced NFAT activation and pressure overload-induced cardiac hypertrophy in mice (22). Thus, inhibition of TRPC3-containing multimeric channels may represent a novel therapeutic strategy for preventing cardiac hypertrophy.

Phosphorylation of TRPC channels has been reported to modulate channel activity (23–25). For example, Fyn, an Src family Tyr kinase, physically interacts with the N-terminal region of TRPC6 proteins, and Tyr phosphorylation of TRPC6 enhances its channel activity (23). It has also been demonstrated that Src-dependent Tyr phosphorylation of TRPC3 is essential for DAG-activated cation influx (24). In contrast, Ser/Thr phosphorylation of TRPC3 channel attenuates its channel activity (25). Activation of PKG is known to regulate $[Ca^{2+}]_i$ at multiple levels (26). PKG activation by a NO donor or cGMP analog has been reported to inhibit voltage-dependent L-type Ca^{2+} channels by α_1-adrenergic receptor stimulation in cardiomyocytes (27). Several reports have shown that TRPC3 and TRPC6 channel activities are greatly attenuated by PKG-catalyzed phosphorylation of TRPC6 at threonine 69 (Thr^{69}) and TRPC3 at Thr^{11} and Ser^{263} (25, 28). The physiological importance of negative regulation of TRPC6 channels by the NO-

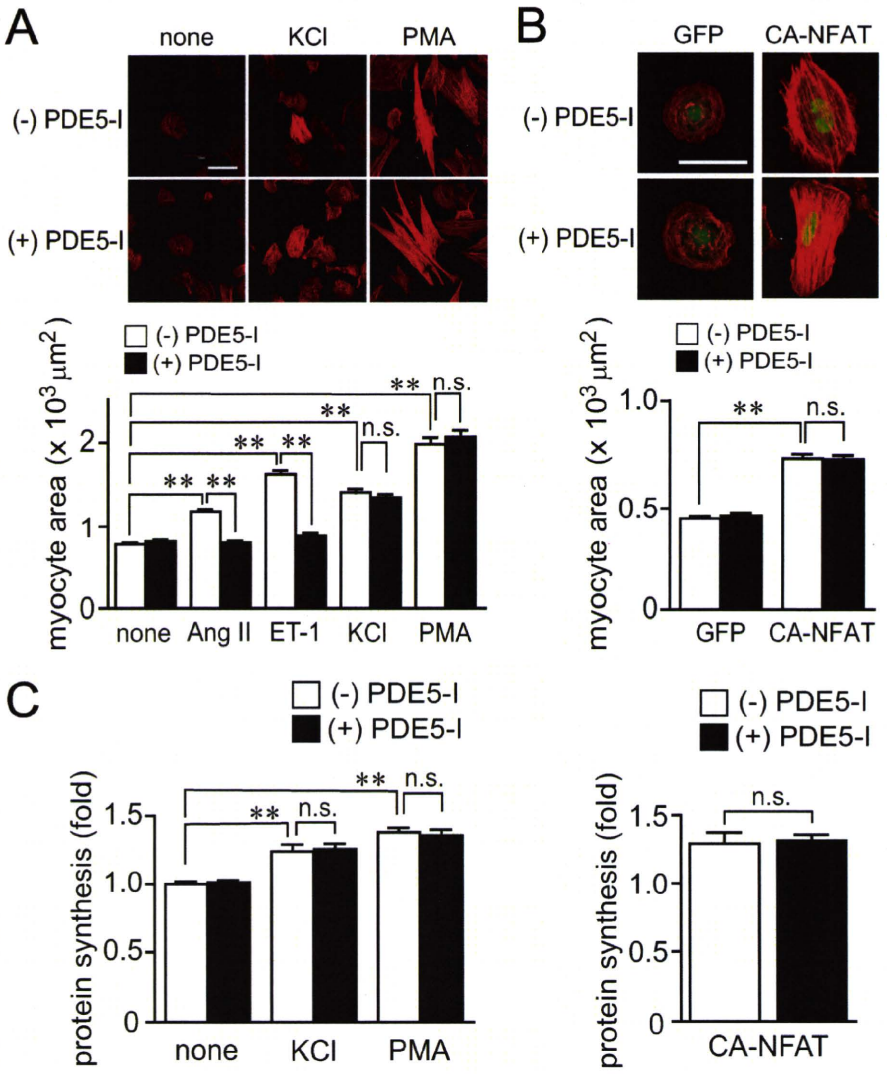

FIGURE 2. **Inhibition of PDE5 does not suppress the agonist-independent cardiomyocyte hypertrophic responses.** *A* and *C*, effects of PDE5-I on hypertrophic responses (actin reorganization, protein synthesis, and increases in area of cardiomyocytes) induced by KCl and phorbol 12-myristrate 13-acetate (*PMA*). Cardiomyocytes were stimulated with Ang II (1 μM), ET-1 (100 nM), KCl (5 mM), or phorbol 12-myristrate 13-acetate (1 μM) for 48 h. *B* and *C*, effects of PDE5-I on hypertrophic growth (*B*) and protein synthesis (*C*) in green fluorescent protein- and CA-NFAT-expressing cardiomyocytes. *Scale bar*, 50 μm. **, $p < 0.01$; *n.s.*, no significance.

cGMP-protein kinase G (PKG) signaling pathway has been reported in vascular smooth muscle cells (28). However, the role of PKG-dependent negative regulation of TRPC6 channels in the heart is still unknown.

Inhibition of cGMP-dependent phosphodiesterase 5 (PDE5) enhances basal PKG activity through an increase in intracellular cGMP concentration. In fact, chronic treatment with sildenafil, a PDE5 inhibitor, exhibits the anti-hypertrophic effects in mice (29, 30) and in patients with systolic heart failure (31). It has been reported that RGS2 mediates cardiac compensation to pressure overload and anti-hypertrophic effects of PDE5 inhibition in mice (32). Because PKG-dependent phosphorylation of RGS2 enhances GTPase activity of the α-subunit of G_q protein ($G\alpha_q$), this may explain the cGMP-dependent disruption of intracellular Ca^{2+} signaling induced by G_q-coupled receptor stimulation. However, we here found that inhibition of PDE5 also suppresses Ca^{2+} responses induced by the DAG analog and mechanical stretch (which may not require the activation of $G\alpha_q$ signaling) in rat neonatal cardiomyocytes. We also demonstrate that inhibition of PDE5 actually induces phosphorylation of TRPC6 proteins at Thr^{69}, leading to inhibition of TRPC6-mediated Ca^{2+} signaling. These results suggest that PKG-dependent inhibition of TRPC6 channel activity is required for the anti-hypertrophic effects of PDE5 inhibition.

EXPERIMENTAL PROCEDURES

Materials and Cell Cultures—A PDE5-selective inhibitor (PDE5-I; 4-{[3′,4′-(methylenedioxy)benzyl]amino}-6-methoxyquinazoline), 4-methyl-4′-[3,5-bis(trifluoromethyl)-1H-pyrazol-1-yl]-1,2,3-thiadiazole-5-carboxanilide (BTP2), and KT5823 were purchased from Calbiochem. 8-Bromo-cGMP (8-Br-cGMP), phorbol 12-myristrate 13-acetate, *S*-nitroso-*N*-acetyl-DL-penicillamine, 1-oleoyl-2-acetyl-*sn*-glycerol (OAG), and ET-1 were from Sigma. Ang II was from Peptide Lab. Fura2/AM was from Dojindo. Bis(1,3-dibutylbarbituric acid)trimethine oxonol ($DiBAC_4(3)$) was from Molecular Probes. Collagenase and Fugene 6 were from Roche Applied Science. Stealth small interfering RNA (siRNA) oligonucleotides, Alexa Fluor 568 phalloidin, and Lipofectamine 2000 were purchased from Invitrogen. Revatio (sildenafil citrate) was from Pfizer. The cDNAs coding a dominant negative mutant of TRPC6 (DN-TRPC6) and the TRPC6 (T69A) mutant were constructed as described (21, 28). Anti-TRPC6 was from Alomone. Phospho-Thr^{69} TRPC6 antiserum was generated against phospho-TRPC6 peptide (CHRRQ(P)TILREK). The phospho-TRPC6 antibody was purified by an antigen column. Isolation of rat neonatal cardiomyocytes and adenoviral infection of LacZ, green fluorescent protein, wild type (WT) TRPC6, or DN-TRPC6 were described (33). For knockdown of rat RGS proteins, cells were transfected with siRNAs (100 nM each) for RGS2 (AGAAAUAGCUCAAACGGGUCUUCCA) and RGS4 (UUUGAAAGCUGCCAGUCCACAUUCA) or control scrambled siRNAs for RGS2 (UUCACGGAACCGACCUUAAAUA) and RGS4 (AAAUAGCGUCUGACCACCCUUAGGU), using Lipofectamine 2000 for 72 h.

Reporter Activity—Measurement of NFAT-dependent luciferase activity and brain natriuretic peptide (BNP) promoter activity was performed as described previously (21). Briefly, cardiomyocytes (5×10^5 cells) plated on 24-well

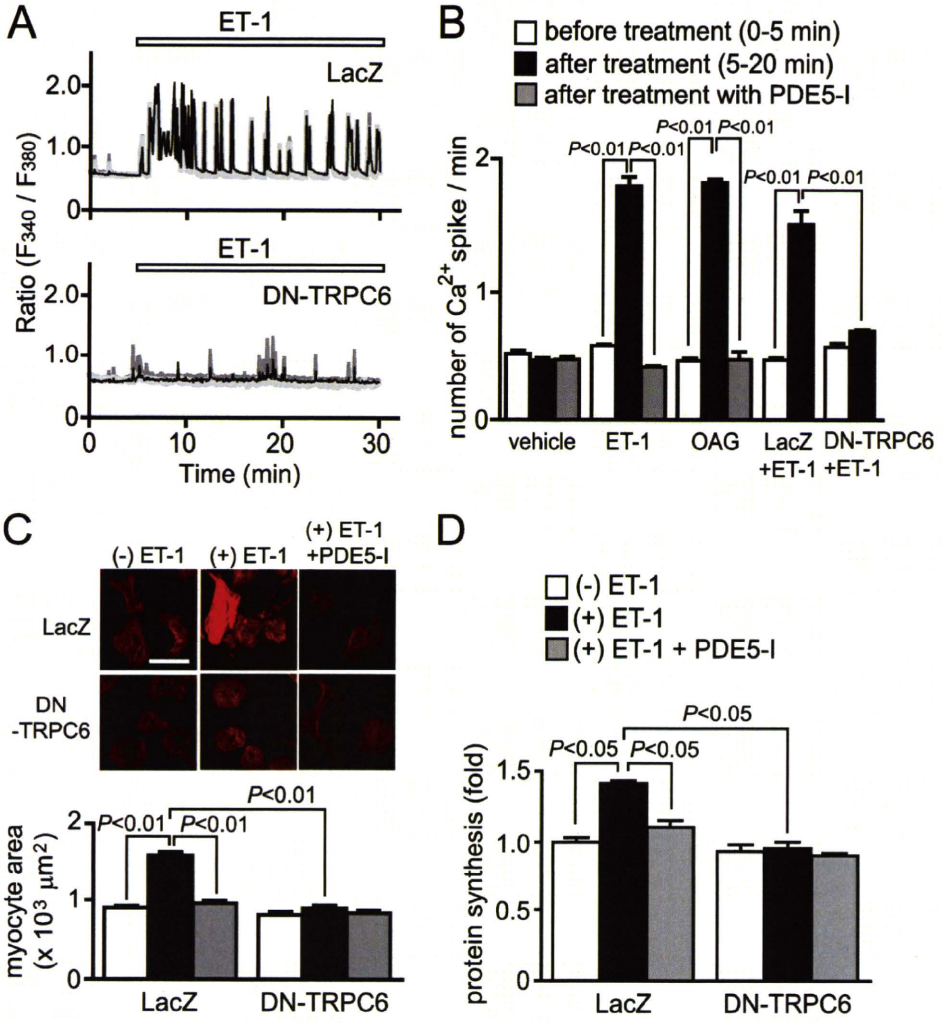

FIGURE 3. **TRPC6 mediates ET-1-induced cardiomyocyte hypertrophic responses.** *A*, Ca^{2+} responses induced by ET-1 (100 nM) in LacZ- and DN-TRPC6-overexpressing cardiomyocytes. *B*, results of the frequency of Ca^{2+} oscillations induced by ET-1 or OAG (30 μM). Cardiomyocytes were pretreated with PDE5-I (10 μM) 35 min before agonist stimulation. *C* and *D*, effects of DN-TRPC6 on ET-1-induced actin reorganization and increase in cell size (*C*) and protein synthesis (*D*). *Scale bar*, 50 μm.

dishes were transiently co-transfected with 0.45 μg of pNFAT-Luc and 0.05 μg of pRL-SV40 control plasmid or with 0.3 μg of pBNP-Luc and 0.2 μg of pRL-SV40 using Fugene 6. Expression of the constitutively active mutant of green fluorescent protein-fused NFAT proteins (CA-NFAT) was performed as described (34). Forty-eight h after transfection, cells were stimulated with Ang II (1 μM), ET-1 (100 nM), or mechanical stretch (21) for 6 h (for NFAT) or 24 h (for BNP).

Measurement of $[Ca^{2+}]_i$ and Membrane Potential—The intracellular Ca^{2+} concentration ($[Ca^{2+}]_i$) of cardiomyocytes or HEK293 cells was determined as described (35, 36). Briefly, HEK293 cells were transfected for 48 h with vector (pCI-neo), WT TRPC6, or TRPC6 (T69A) mutant using Fugene 6. Cardiomyocytes (1×10^6 cells) were plated on gelatin-coated glass bottom 35-mm dishes or on laminin-coated silicone rubber culture dishes (4 cm^2; STREX) and were loaded with 1 μM fura-2/AM at 37 °C for 30 min (37). As we measured the changes in $[Ca^{2+}]_i$ of the same cells before and after mechanical stretch, we treated cells with 20% of transient stretch for 3 s using automatic stretch systems (STB-150; STREX). Measurement and analysis of membrane potential were performed using $DiBAC_4(3)$ as described (21). The fluorescence intensity was measured with a video image analysis system (Aquacosmos, Hamamatsu Photonics).

Animal Models and Drug Treatment—All experiments on male C57BL6/J mice (C57BL6/J) were performed in accordance with the Guide for the Care and Use of Laboratory Animals prepared by Kyushu University. Sildenafil (100 mg/kg/day) was orally administered once a day for 1 week, and then hearts were removed and homogenized with radioimmune precipitation buffer.

Western Blot Analysis—TRPC6-expressing HEK293 cells (3×10^5 cells) or cardiomyocytes (1×10^6 cells) plated on 6-well dishes were directly harvested with 2× SDS sample buffer (200 μl). After centrifugation, supernatants (20–40 μl) were fractionated by 8% SDS-polyacrylamide gel and then transferred onto polyvinylidene difluoride membrane. For measurement of TRPC6 phosphorylation in mouse hearts, supernatants (100 μg of proteins) without boiling treatment were applied onto SDS-polyacrylamide gel. The expression and phosphorylation of endogenous TRPC6 proteins were detected by anti-TRPC6 (dilution rate, 1:1000) and anti-phospho-TRPC6 (1:1000) antibodies. We visualized the reactive bands using Supersignal® West Pico Luminol/Enhancer solution (Pierce). The optical density of the film was scanned and measured with Scion Image software.

Measurement of Hypertrophic Responses of Cardiomyocytes—Measurement of cardiomyocyte hypertrophy was performed as described (21, 34). Cardiomyocytes were fixed by paraformaldehyde and then stained with Alexa Fluor 548 phalloidin to visualize actin filaments. Digital photographs were taken at ×600 magnification with confocal microscopy (FV-10i, Olympus) or a Biozero microscope (BZ-8000, Keyence), and the average values of the cardiomyocyte area ($n > 100$ cells) were calculated using a BZ-II analyzer (Keyence). Protein synthesis was measured by [^{3}H]leucine incorporation. After cells were stimulated with Ang II or ET-1 for 2 h, [^{3}H]leucine (1 μCi/ml) was added to the culture medium and further incubated for 6 h. The incorporated [^{3}H]leucine was measured using a liquid scintillation counter.

Statistical Analysis—The results are shown as means ± S.E. All experiments were repeated at least three times. Statisti-

cal comparisons were made with a two-tailed Student's *t* test or analysis of variance followed by the Student-Newman-Keuls procedure with significance imparted at p values of <0.05.

RESULTS

Suppression of Diacylglycerol-mediated Ca^{2+} Responses by Inhibition of PDE5—We first investigated whether inhibition of PDE5 suppresses agonist-induced Ca^{2+} responses and hypertrophic responses in rat cardiomyocytes. Treatment with PDE5-I completely suppressed Ang II- or ET-1-induced hypertrophic responses, such as an increase in cell size, actin reorganization, hypertrophic gene (BNP) expression, and protein synthesis (Fig. 1, *A–C*). Stimulation of cardiomyocytes with ET-1 increases the frequency of Ca^{2+} oscillations through voltage-dependent Ca^{2+} channels (38). PDE5-I also suppressed ET-1-induced NFAT activation and oscillatory and sustained increase in $[Ca^{2+}]_i$ (Fig. 1, *D* and *E*). Although expression of CA-NFAT increased NFAT activity about 2.5-fold, this NFAT activation was not suppressed by PDE5-I (data not shown). These results suggest that PDE5-I inhibits NFAT activity through inhibition of Ca^{2+} responses. We have previously shown that DAG-sensitive TRPC channels (TRPC3 and TRPC6) mediate Ang II-induced activation of voltage-dependent Ca^{2+} influx through membrane depolarization (21). Treatment with OAG increased NFAT activity and the frequency of Ca^{2+} spikes, which were suppressed by PDE5-I (Fig. 1, *D* and *F*). In addition, the OAG-induced membrane depolarization, as determined by $DiBAC_4(3)$ imaging, was completely suppressed by PDE5-I pretreatment (Fig. 1*G*). Furthermore, nitrendipine-sensitive voltage-dependent Ca^{2+} influx-mediated increase in $[Ca^{2+}]_i$ induced by high KCl was not affected by PDE5-I pretreatment (Fig. 1*H*). In addition, the hypertrophic responses induced by high KCl (Fig. 2, *A* and *C*) or the expression of CA-NFAT (Fig. 2*B*) were not suppressed by PDE5 inhibition. Although DAG also activates protein kinase C-dependent hypertrophic signaling pathway (3), PDE5-I did not suppress the phorbol 12-myristrate 13-acetate-induced hypertrophic responses (Fig. 2, *A* and *C*). These results suggest that PDE5-I suppresses agonist-induced Ca^{2+} responses and cardiomyocyte hypertrophy through inhibition of DAG-mediated membrane depolarization.

Inhibition of TRPC6 Channel Activity by PDE5 Inhibition—To investigate the involvement of TRPC6 in agonist-induced cardiomyocyte hypertrophy, we used DN-TRPC6 (21). As shown in Fig. 3*A*, treatment of cardiomyocytes with ET-1 or OAG significantly increased the frequency of Ca^{2+} spikes, which were completely suppressed by PDE5 inhibition (Fig. 3, *A* and *B*). Expression of DN-TRPC6 also completely suppressed ET-1-induced increases in the frequency of Ca^{2+} spikes (Fig. 3, *A* and *B*) and hypertrophic responses (Fig. 3, *C* and *D*). The anti-hypertrophic effect of PDE5-I was completely abolished in DN-TRPC6-expressing myocytes, suggesting that PDE5-I suppresses the TRPC6-mediated hypertrophic signaling pathway.

Takahashi *et al.* (28) have recently reported that activation of the NO-cGMP-PKG pathway by extracellular treatment with a NO donor or cGMP analog inhibits TRPC6 channel activity through phosphorylation of TRPC6 at Thr^{69}. Thus,

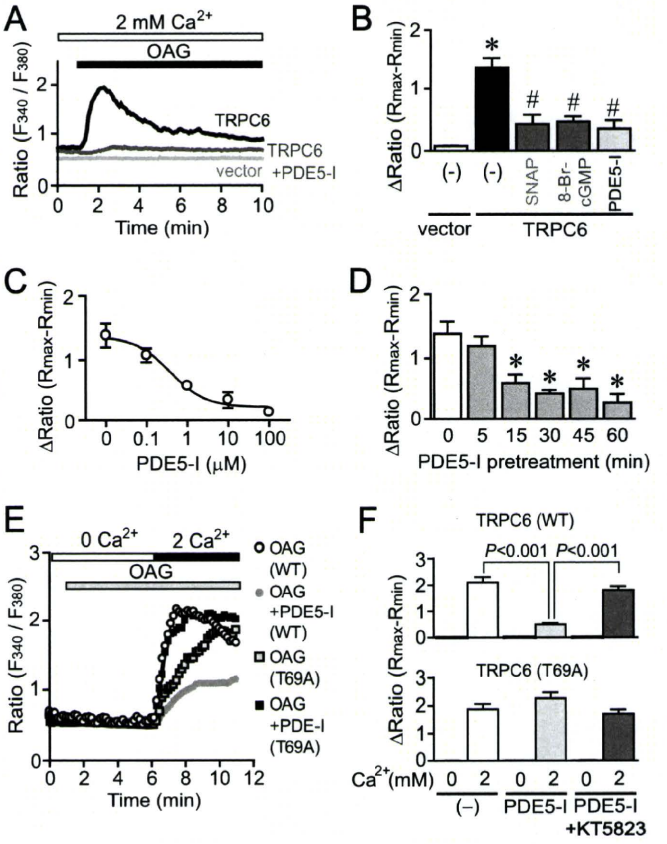

FIGURE 4. **PKG-dependent suppression of TRPC6-mediated Ca^{2+} influx by PDE5 inhibition.** *A*, average time courses of Ca^{2+} responses induced by OAG (30 μM) in vector and TRPC6-expressing HEK293 cells with or without PDE5-I. *B*, peak increases in $[Ca^{2+}]_i$ induced by OAG in vector- and TRPC6-expressing cells. HEK293 cells were treated with *S*-nitroso-*N*-acetyl-DL-penicillamine (*SNAP*) (100 μM), 8-Br-cGMP (100 μM), or PDE5-I (10 μM) for 30 min before the addition of OAG (30 μM). *C* and *D*, concentration-dependent (*C*) and time-dependent (*D*) suppression of OAG-induced $[Ca^{2+}]_i$ increases by PDE5-I. *E* and *F*, effects of PDE5-I on OAG-induced Ca^{2+} influx-mediated $[Ca^{2+}]_i$ increases in TRPC6 (WT)- and TRPC6 (T69A)-expressing cells. HEK293 cells were treated with KT5823 (1 μM) for 30 min before the addition of OAG. *, $p < 0.05$ *versus* vector (*white bar*); #, $p < 0.05$ *versus* TRPC6 (−) control (*black bar*).

we next examined whether PDE5 inhibition attenuates TRPC6 channel activity. Compared with vector-expressing HEK293 cells, treatment with OAG induced a marked increase in $[Ca^{2+}]_i$ of TRPC6-expressing cells (Fig. 4*A*). The TRPC6-mediated increase in $[Ca^{2+}]_i$ was significantly suppressed by pretreatment with PDE5-I as well as *S*-nitroso-*N*-acetyl-DL-penicillamine and 8-Br-cGMP (Fig. 4*B*). The IC_{50} value of inhibition of the TRPC6-mediated increase in $[Ca^{2+}]_i$ by PDE5-I was 0.41 ± 0.08 μM (Fig. 4*C*). More than 15 min of pretreatment with PDE5-I was required for the suppression of the TRPC6-mediated increase in $[Ca^{2+}]_i$ induced by OAG (Fig. 4*D*). PDE5-I suppressed the Ca^{2+} influx-mediated increase in $[Ca^{2+}]_i$ induced by OAG in TRPC6 (WT)-expressing cells, which was completely abolished by co-treatment with a PKG-selective inhibitor, KT5823 (Fig. 4, *E* and *F*). These results suggest that activation of PKG is required for the inhibition of TRPC6 channel activity. In fact, the suppression of OAG-induced Ca^{2+} influx by PDE5-I treatment was abolished in TRPC6 (T69A)-expressing cells. Thus, PKG-dependent phosphorylation of TRPC6 at Thr^{69} may be essential for inhibition of TRPC6 channel activity by PDE5 inhibition.

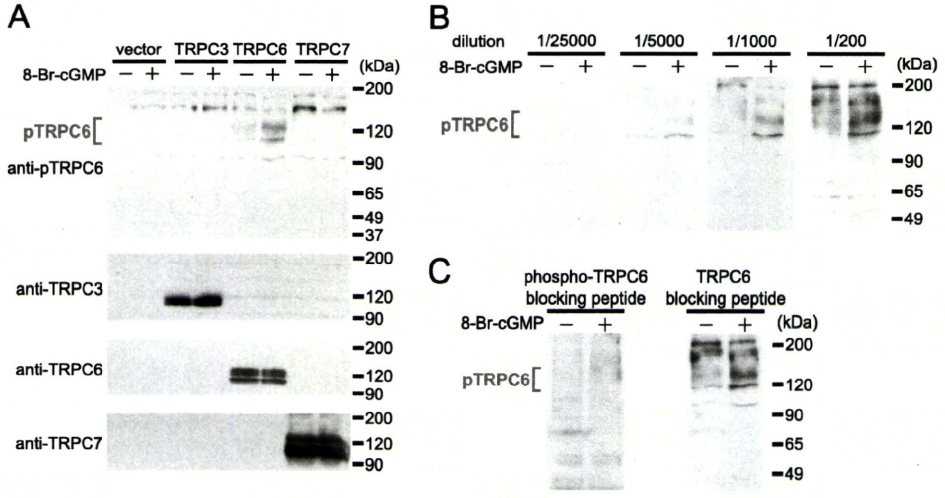

FIGURE 5. **Specific recognition of TRPC6 phosphorylation at Thr^{69} by a phospho-specific antibody.** *A*, phosphorylation of TRPC6 at Thr^{69} induced by PKG activation in vector-, TRPC3-, TRPC6-, and TRPC7-expressing HEK293 cells. HEK293 cells were treated with 8-Br-cGMP (100 μM) for 2 h. *B*, optimization of dilution of anti-phospho-TRPC6 antibody. Antibody (0.56 mg/ml) was diluted with Tris-buffered saline plus 0.1% Tween 20 (TBS-T) and incubated with blots for 1 h at room temperature. *C*, effect of treatment with a TRPC6-blocking peptide on the recognition of TRPC6 phosphorylation by this antibody. Blots were incubated with phospho-TRPC6 antibody diluted 1:1000 in TBS-T with phospho-TRPC6-blocking peptide or non-phosphorylated TRPC6-blocking peptide (10 μg/ml) for 1 h at room temperature.

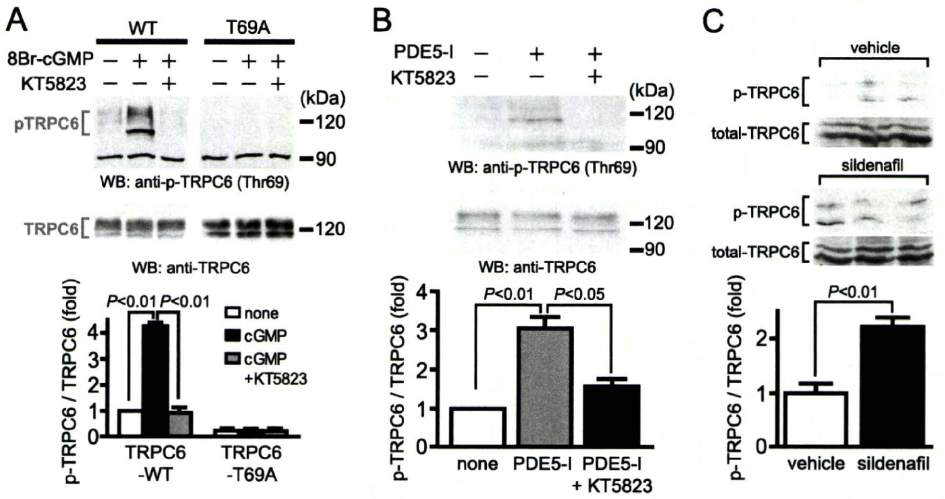

FIGURE 6. **PKG-dependent phosphorylation of Thr^{69} in TRPC6 by PDE5 inhibition.** *A*, PKG-dependent phosphorylation of TRPC6 proteins at Thr^{69} in TRPC6 (WT)- and TRPC6 (T69A)-expressing HEK293 cells. HEK293 cells were treated with KT5823 (1 μM) for 20 min before the addition of 8-Br-cGMP (100 μM) and PDE5-I (10 μM) for 30 min. *B*, PKG-dependent TRPC6 phosphorylation by PDE5-I. Cardiomyocytes were treated with KT5823 for 20 min before the addition of PDE5-I (10 μM) for 1 h. *C*, effects of sildenafil on the phosphorylation of TRPC6 in mice. One week after oral administration with sildenafil (100 mg/kg/day), hearts were lysed with radioimmune precipitation buffer, and 100 μg of proteins were applied to SDS-PAGE.

Phosphorylation of TRPC6 Proteins at Thr^{69} by PDE5 Inhibition—In order to examine whether inhibition of PDE5 actually induces phosphorylation of TRPC6 proteins in cardiomyocytes, we generated a phospho-specific TRPC6 (Thr^{69}) antibody. Because TRPC6 proteins have two glycosylation sites (39), a single 100 kDa band and smear 110–120 kDa bands due to several patterns of glycosylation were observed in TRPC6 wild type (WT)-overexpressing HEK293 cells (Fig. 5*A*). Phosphorylation of TRPC6 proteins was observed only when HEK293 cells were stimulated with 8-Br-cGMP. In contrast, this phosphorylation was not observed in vector-, TRPC3-, or TRPC7-expressing HEK293 cells, even when cells were stimulated with 8-Br-cGMP. The TRPC6 phosphorylation could be detectable when the antibody was diluted from 1,000- to 5,000-fold (Fig. 5*B*). Furthermore, the TRPC6 phosphorylation bands were completely abolished by the treatment with phospho-TRPC6-blocking peptide but not by control blocking peptide (Fig. 5*C*). These results clearly suggest that our phospho-specific TRPC6 antibody specifically recognized the phosphorylation of rodent TRPC6 at Thr^{69}.

Activation of PKG by 8-Br-cGMP and PDE5-I stimulated the phosphorylation of TRPC6 proteins, which was completely suppressed by the treatment with KT5823 in TRPC6-WT-expressing HEK293 cells (Fig. 6, *A* and *B*). The PKG-mediated TRPC6 phosphorylation was not observed in TRPC6 (T69A)-expressing cells, indicating the specificity of this antibody. Treatment with PDE5-I significantly increased the phosphorylation of native TRPC6 proteins in rat cardiomyocytes, which was completely suppressed by KT5823 (Fig. 6*B*). We further examined whether inhibition of PDE5 actually phosphorylates TRPC6 proteins *in vivo*. Takimoto *et al.* (29) have previously reported that chronic treatment with sildenafil (100 mg/kg/day) prevents and reverses cardiac hypertrophy induced by pressure overload in mice. We found that oral treatment with sildenafil (100 mg/kg/day) for 1 week, under the same conditions as in their report, actually increases TRPC6 phosphorylation levels in mouse hearts (Fig. 6*C*).

Inhibition of TRPC6 Phosphorylation at Thr^{69} Diminishes the Anti-hypertrophic Effects of PDE5 Inhibition—Overexpression of TRPC6 (T69A) enhanced the increase in NFAT activity and BNP expression induced by ET-1, which was not suppressed by PDE5-I (Fig. 7, *A* and *B*). In addition, expression of TRPC6 (WT) or TRPC6 (T69A) enhanced the ET-1-induced hypertrophic responses of cardiomyocytes (Fig. 7, *C* and *D*). Although PDE5-I completely suppressed the ET-1-induced hypertrophic responses in control (vector)- or TRPC6 (WT)-expressing cardiomyocytes, PDE5-I did not suppress hypertrophic responses in TRPC6 (T69A)-expressing cardiomyocytes. These results suggest that inhibition of TRPC6 channel activity via its PKG-dependent phosphorylation at Thr^{69} participates in anti-cardiomyocyte hypertrophic effects of PDE5 inhibition.

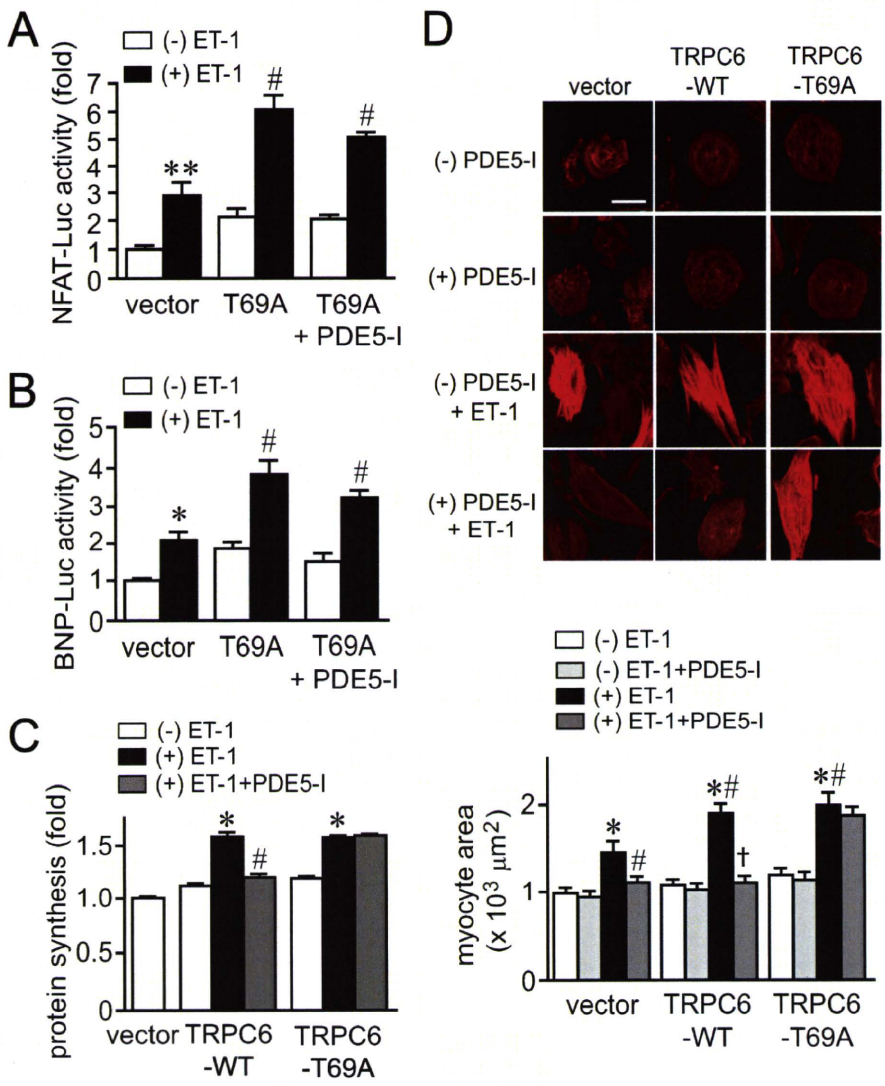

FIGURE 7. **Phosphorylation of Thr^{69} is essential for the anti-hypertrophic effects of PDE5 inhibition.** *A* and *B*, effects of PDE5-I on ET-1-induced NFAT activation (*A*) and BNP gene expression (*B*) in TRPC6 (T69A)-expressing cardiomyocytes. *C* and *D*, effects of PDE5-I on the ET-1-induced protein synthesis (*C*) and increase in the size of TRPC6 (T69A)-overexpressing cardiomyocytes (*D*). Cardiomyocytes were treated with PDE5-I (10 μM) for 20 min before the addition of ET-1 (100 nM). *Scale bar*, 50 μm. *, $p < 0.05$; **, $p < 0.01$ *versus* without (−) ET-1 within vector. #, $p < 0.05$ *versus* vector with (+) ET-1. †, $p < 0.01$ *versus* TRPC6-WT with ET-1.

Suppression of Mechanical Stretch-induced Ca^{2+} Responses by PDE5 Inhibition—Because mechanical stress is also involved in the development of cardiac hypertrophy, we next examined whether PDE5-I inhibits Ca^{2+} responses induced by mechanical stretch. In control cardiomyocytes, a periodic increase in $[Ca^{2+}]_i$ was observed after cells were stretched by 20% for 3 s with a speed of 20 mm/s (Fig. 8*A*). A bis(triluoromethyl)pyrazole derivative, BTP2, is recently used as a selective inhibitor of the TRPC1 to -7 channels. We previously reported that BTP2 at 3 μM suppresses TRPC6-mediated Ca^{2+} influx by 80% in HEK293 cells (22). Treatment with PDE5-I or BTP2 abolished mechanical stretch-induced increase in $[Ca^{2+}]_i$ (Fig. 8*A*). Mechanical stretch-induced increases in NFAT-dependent luciferase activity, BNP-luciferase activity, and protein synthesis were suppressed by PDE5-I, which was canceled by co-treatment with KT5823 (Fig. 8, *B–D*). We also found that mechanical stretch-induced increases in $[Ca^{2+}]_i$, NFAT activation, and hypertrophic responses were completely suppressed by the expression of DN-TRPC6 (Fig. 8, *B–D*). These results suggest that PDE5-I suppresses mechanical stretch-induced Ca^{2+} responses linked to cardiomyocyte hypertrophic responses through inhibition of TRPC6 channels.

Knockdown of RGS2 and RGS4 Does Not Affect the Effect of PDE5-I—It has been recently reported that PKG-dependent phosphorylation of RGS2 and RGS4 mediates the anti-hypertrophic effects in mouse hearts (32, 40, 41). Thus, we next examined the involvement of RGS proteins in the inhibition of agonist-induced Ca^{2+} responses by PDE5 inhibition, using siRNAs for RGS2 and RGS4. We confirmed that the treatment of cardiomyocytes with siRNAs for RGS2/4 reduced the expression levels of RGS2 and RGS4 mRNAs to 18.5 ± 5.2 and 26.7 ± 7.8%, respectively. Knockdown of RGS2/4 proteins did not affect Ca^{2+} responses and NFAT activation induced by ET-1 (Fig. 9). The addition of extracellular Ca^{2+} induced a Ca^{2+} influx-mediated increase in $[Ca^{2+}]_i$ by ET-1 stimulation, which was significantly suppressed by PDE5-I treatment in control myocytes (Fig. 9, *A–C*). The Ca^{2+} influx-mediated $[Ca^{2+}]_i$ increases and increase in NFAT activity by agonist stimulation were slightly enhanced in RGS2/4-deficient myocytes and were also significantly suppressed by PDE5-I treatment (Fig. 9, *B–D*). These results suggest that RGS2 and RGS4 proteins are not mainly involved in the inhibition of agonist-induced Ca^{2+} responses by PDE5 inhibition in cardiomyocytes.

DISCUSSION

In this study, we have demonstrated that inhibition of PDE5 suppresses agonist-induced and mechanical stretch-induced hypertrophic responses in rat cardiomyocytes. The increases in the frequency of Ca^{2+} oscillations induced by OAG or mechanical stretch are greatly attenuated by PDE5 inhibition. PDE5-I suppresses OAG-induced membrane depolarization, suggesting the inhibition of DAG-sensitive TRPC channels by PDE5 inhibitor. Treatment with PDE5-I actually induces PKG-dependent phosphorylation of TRPC6 proteins at Thr^{69} and inhibits TRPC6-mediated Ca^{2+} responses. Because the inhibition of ET-1-induced hypertrophic responses by PDE5-I was abolished in TRPC6 (T69A)-expressing cardiomyocytes, we suggest that phosphorylation of TRPC6 is required for

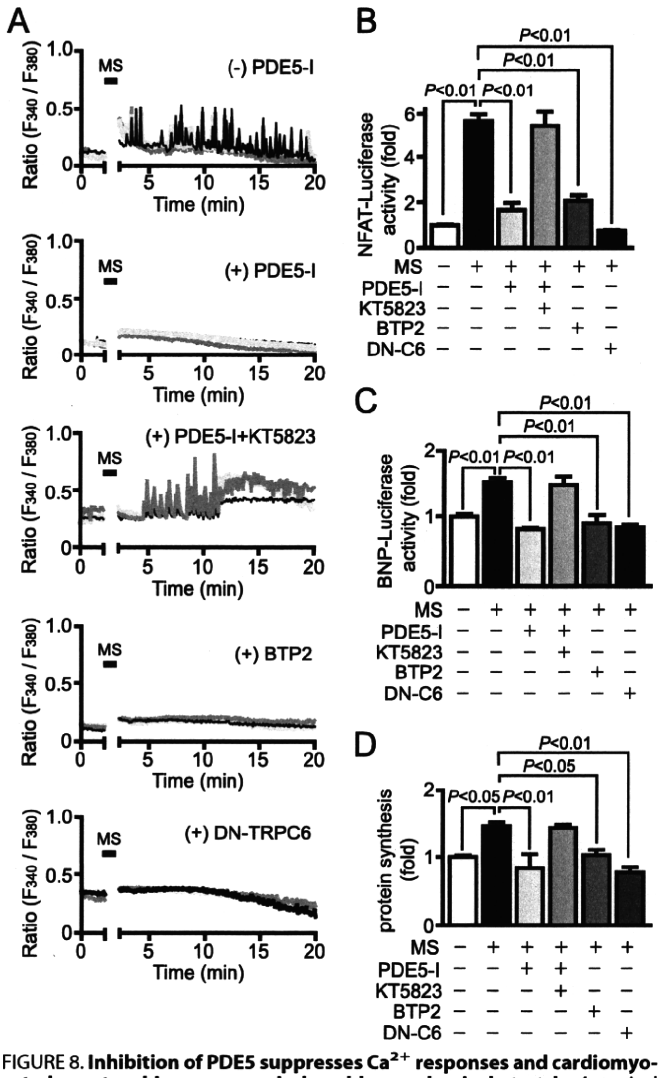

FIGURE 8. **Inhibition of PDE5 suppresses Ca^{2+} responses and cardiomyocyte hypertrophic responses induced by mechanical stretch.** *A*, typical traces of Ca^{2+} responses induced by mechanical stretch (*MS*) in the absence or presence of PDE5-I, KT5823, or BTP2. Cardiomyocytes were treated with PDE5-I (10 μM) or BTP2 (5 μM) for 35 min before MS. DN-TRPC6 proteins were expressed using adenoviral infection. *B–D*, effects of PDE5-I, BTP2, and DN-TRPC6 on the MS-induced NFAT activation (*B*) and hypertrophic responses (BNP gene expression (*C*) and protein synthesis (*D*)).

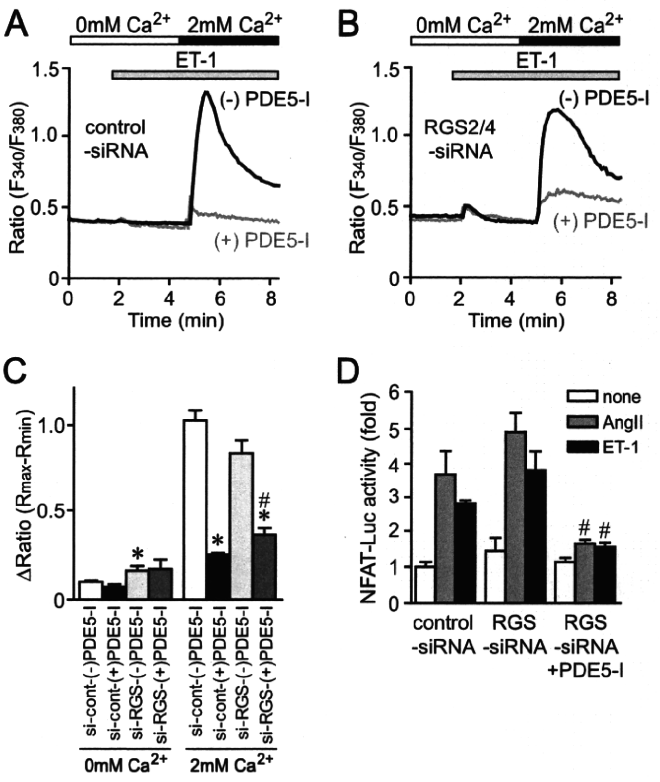

FIGURE 9. **PDE5-I suppresses ET-1-induced Ca^{2+} responses in RGS2/4-down-regulated cardiomyocytes.** *A* and *B*, average time courses of Ca^{2+} responses induced by ET-1 in the absence or presence of PDE5-I in control siRNA-treated cardiomyocytes (*A*) and RGS2/4 siRNAs-treated cardiomyocytes (*B*). *C*, peak Ca^{2+} releases (0 mM Ca^{2+}) and Ca^{2+} influx-mediated increases in $[Ca^{2+}]_i$ (2 mM Ca^{2+}) induced by ET-1 (100 nM). *D*, effects of knockdown of RGS2/4 proteins on PKG-dependent inhibition of ET-1-induced NFAT activation by PDE5-I. *, $p < 0.05$ *versus* control siRNA-treated cardiomyocytes without PDE5-I; #, $p < 0.05$ *versus* RGS2/4 siRNA-treated cardiomyocytes without PDE5-I.

the anti-hypertrophic effects of PDE5 inhibition. In addition, PDE5-I-induced suppression of Ca^{2+} influx induced by ET-1 was not abolished by the knockdown of RGS2 and RGS4, both of which are reported to be activated by PKG. This result emphasizes the physiological importance of TRPC6 phosphorylation by PDE5-I in suppressing Ca^{2+} influx induced by agonist stimulation and mechanical stretch.

Higazi *et al.* (38) has recently reported that inositol-1,4,5-trisphosphate-induced Ca^{2+} release from perinuclear inositol-1,4,5-trisphosphate receptors by ET-1 stimulation or membrane depolarization preferentially couples to the calcineurin/NFAT pathway to induce hypertrophy. They have also demonstrated that the potentiation of Ca^{2+} influx activity induced by isoproterenol or BayK8644 induces activation of calcineurin/NFAT signaling pathway via Ca^{2+} release from perinuclear inositol-1,4,5-trisphosphate receptors. This mechanism may be involved in the process of voltage-dependent Ca^{2+} influx-mediated NFAT activation evoked by TRPC6 activation. Although we did not measure nuclear Ca^{2+} concentrations, PDE5-I may inhibit the increase in nuclear Ca^{2+} concentrations because PDE5-I suppresses NFAT activation induced by ET-1.

Because PDE5-I did not suppress the high KCl-induced increase in $[Ca^{2+}]_i$ (Fig. 1), we suggest that PKG activation by PDE5-I does not inhibit L-type Ca^{2+} channels. In contrast, Fiedler *et al.* (27) have reported that overexpression of PKG type I suppresses single L-type Ca^{2+} channel open probability and $[Ca^{2+}]_i$ transient amplitude. This discrepancy can be explained by the intensity of PKG activation. Although we show that PDE5-I increased the TRPC6 phosphorylation level about 3-fold, the treatment with 8-Br-cGMP induced a more than 5-fold increase in TRPC6 phosphorylation level (data not shown). This suggests that PDE5-I moderately activates PKG, and this activation is insufficient to inhibit L-type Ca^{2+} channel activity.

Inhibition of PDE5 suppresses mechanical stretch-induced Ca^{2+} responses in cardiomyocytes. Because the pattern of Ca^{2+} spikes is similar to those induced by ET-1 or OAG stimulation, membrane depolarization may be also involved in this mechanism. This idea is supported by the reports that DAG-sensitive TRPC channels work as stretch-

activated depolarizing channels in the vascular system (42–44). It has recently been reported that TRPC6 is activated by mechanical stretch through two pathways: G protein-mediated indirect activation and direct activation of TRPC6 (42). Furthermore, TRPC6 can be synergistically activated by mechanical force in the presence of G_q-coupled receptor stimulation (43). We have previously reported that mechanical stretch increases the concentration of extracellular nucleotides, which stimulate G_q protein-coupled P2Y receptors (37). Thus, extracellular nucleotides released by mechanical stretch and mechanical force may synergistically increase TRPC6 channel activity in rat neonatal cardiomyocytes.

Because Kwan *et al.* (25) reported that the activation of PKG by NO donor and 8-Br-cGMP increases phosphorylation at Thr^{11} and Ser^{263} of human TRPC3 proteins, it is possible that inhibition of PDE5 also results in phosphorylation of TRPC3 proteins and reduction of TRPC3 channel activity. Although Ser^{263} of human TRPC3 protein is conserved among humans, rats, and mice, Thr^{11} is not present in mouse and rat TRPC3 proteins. We have tried to generate an antibody to recognize the phosphorylated form of Ser^{263} in TRPC3 but failed to obtain the useful antibody. However, we confirmed that PDE5-I inhibits its TRPC3-mediated Ca^{2+} influx induced by OAG in TRPC3-expressing HEK293 cells, which was abolished in TRPC3 (S325A)-expressing HEK293 cells ($n = 2$; data not shown). Because the Ser^{325} in mouse TRPC3 protein is identical to Ser^{263} in human TRPC3 protein, this result implies that the inhibition of TRPC3 channel activity by PDE-I may also be involved in the anti-hypertrophic effects of PDE5 inhibition.

We have not yet been able to identify the individual roles of TRPC6 and TRPC3 channels in cardiomyocytes. Despite their high degree of structural and functional similarity, TRPC3, TRPC6, and TRPC7 are substantially different in their basal channel activities (45). The basal channel activity of TRPC6 is tightly regulated (39). In contrast, TRPC3 and TRPC7 have considerable constitutive activity when expressed in various cell lines (46). Despite the low basal activity of TRPC6 channels, results from transgenic mice with cardiomyocyte-specific expression of TRPC3 or TRPC6 channels show that the up-regulation of TRPC6 channel proteins is essential for the development of cardiac hypertrophy (13, 14). In pathological conditions, hearts are exposed to mechanical stress and neurohumoral factors. Therefore, a characteristic of TRPC6 channels that is synergistically activated by mechanical stretch in the presence of a low concentration of agonist (43) may explain the mechanism of induction of pathological hypertrophy. Because TRPC3 has high constitutive activity among the DAG-activated TRPC3/6/7 family and is up-regulated in smooth muscle cells from TRPC6-deficient mice (45), the TRPC6-deficient mouse heart may cause excessive hypertrophy by pressure overload like a TRPC3-transgenic mouse heart (13). In addition, there is no pharmacological tool that selectively inhibits TRPC6 channel activity. Generation of transgenic mice with heart-specific expression of the dominant negative TRPC6 mutant, which moderately inhibits the function of TRPC6 channels without any compensation, will be necessary for understanding the pathophysiological role of TRPC6 in the heart.

In conclusion, we demonstrated that inhibition of DAG-sensitive TRPC channel activities through PKG-dependent phosphorylation is required for the anti-hypertrophic effects of PDE5 inhibition in rat cardiomyocytes. Our finding will provide a new insight for the creation of therapeutic strategies for heart failure.

Acknowledgments—We thank Marina Ariyoshi and Shinji Oda for measurement of Ca^{2+} imaging during the early stage of this study. We also thank Dr. Koichiro Kuwahara (Kyoto University) for helpful comments.

REFERENCES

1. Mann, D. L. (1999) *Circulation* **100,** 999–1008
2. Dorn, G. W., 2nd, and Force, T. (2005) *J. Clin. Invest.* **115,** 527–537
3. Heineke, J., and Molkentin, J. D. (2006) *Nat. Rev. Mol. Cell Biol.* **7,** 589–600
4. Liao, X. D., Tang, A. H., Chen, Q., Jin, H. J., Wu, C. H., Chen, L. Y., and Wang, S. Q. (2003) *Biochem. Biophys. Res. Commun.* **310,** 405–411
5. Molkentin, J. D., Lu, J. R., Antos, C. L., Markham, B., Richardson, J., Robbins, J., Grant, S. R., and Olson, E. N. (1998) *Cell* **93,** 215–228
6. Frey, N., McKinsey, T. A., and Olson, E. N. (2000) *Nat. Med.* **6,** 1221–1227
7. Ramirez, M. T., Zhao, X. L., Schulman, H., and Brown, J. H. (1997) *J. Biol. Chem.* **272,** 31203–31208
8. Song, K., Backs, J., McAnally, J., Qi, X., Gerard, R. D., Richardson, J. A., Hill, J. A., Bassel-Duby, R., and Olson, E. N. (2006) *Cell* **125,** 453–466
9. Berridge, M. J., Bootman, M. D., and Roderick, H. L. (2003) *Nat. Rev. Mol. Cell Biol.* **4,** 517–529
10. Colella, M., Grisan, F., Robert, V., Turner, J. D., Thomas, A. P., and Pozzan, T. (2008) *Proc. Natl. Acad. Sci. U.S.A.* **105,** 2859–2864
11. Large, W. A. (2002) *J. Cardiovasc. Electrophysiol.* **13,** 493–501
12. Yao, X., and Garland, C. J. (2005) *Circ. Res.* **97,** 853–863
13. Nakayama, H., Wilkin, B. J., Bodi, I., and Molkentin, J. D. (2006) *FASEB J.* **20,** 1660–1670
14. Kuwahara, K., Wang, Y., McAnally, J., Richardson, J. A., Bassel-Duby, R., Hill, J. A., and Olson, E. N. (2006) *J. Clin. Invest.* **116,** 3114–3126
15. Nishida, M., and Kurose, H. (2008) *Naunyn Schmiedebergs Arch. Pharmacology* **378,** 395–406
16. Bush, E. W., Hood, D. B., Papst, P. J., Chapo, J. A., Minobe, W., Bristow, M. R., Olson, E. N., and McKinsey, T. A. (2006) *J. Biol. Chem.* **281,** 33487–33496
17. Seth, M., Zhang, Z. S., Mao, L., Graham, V., Burch, J., Stiber, J., Tsiokas, L., Winn, M., Abramowitz, J., Rockman, H. A., Birnbaumer, L., and Rosenberg, P. (2009) *Circ. Res.* **105,** 1023–1030
18. Mori, Y., Wakamori, M., Miyakawa, T., Hermosura, M., Hara, Y., Nishida, M., Hirose, K., Mizushima, A., Kurosaki, M., Mori, E., Gotoh, K., Okada, T., Fleig, A., Penner, R., Iino, M., and Kurosaki, T. (2002) *J. Exp. Med.* **195,** 673–681
19. Zagranichnaya, T. K., Wu, X., and Villereal, M. L. (2005) *J. Biol. Chem.* **280,** 29559–29569
20. Hofmann, T., Schaefer, M., Schultz, G., and Gudermann, T. (2002) *Proc. Natl. Acad. Sci. U.S.A.* **99,** 7461–7466
21. Onohara, N., Nishida, M., Inoue, R., Kobayashi, H., Sumimoto, H., Sato, Y., Mori, Y., Nagao, T., and Kurose, H. (2006) *EMBO J.* **25,** 5305–5316
22. Kiyonaka, S., Kato, K., Nishida, M., Mio, K., Numaga, T., Sawaguchi, Y., Yoshida, T., Wakamori, M., Mori, E., Numata, T., Ishii, M., Takemoto, H., Ojida, A., Watanabe, K., Uemura, A., Kurose, H., Morii, T., Kobayashi, T., Sato, Y., Sato, C., Hamachi, I., and Mori, Y. (2009) *Proc. Natl. Acad. Sci. U.S.A.* **106,** 5400–5405
23. Hisatsune, C., Kuroda, Y., Nakamura, K., Inoue, T., Nakamura, T., Michikawa, T., Mizutani, A., and Mikoshiba, K. (2004) *J. Biol. Chem.* **279,** 18887–18894
24. Vazquez, G., Wedel, B. J., Kawasaki, B. T., Bird, G. S., and Putney, J. W., Jr.

(2004) *J. Biol. Chem.* **279,** 40521–40528
25. Kwan, H. Y., Huang, Y., and Yao, X. (2004) *Proc. Natl. Acad. Sci. U.S.A.* **101,** 2625–2630
26. Kass, D. A., Champion, H. C., and Beavo, J. A. (2007) *Circ. Res.* **101,** 1084–1095
27. Fiedler, B., Lohmann, S. M., Smolenski, A., Linnemuller, S., Pieske, B., Schroder, F., Molkentin, J. D., Drexler, H., and Wollert, K. C. (2002) *Proc. Natl. Acad. Sci. U.S.A.* **99,** 11363–11368
28. Takahashi, S., Lin, H., Geshi, N., Mori, Y., Kawarabayashi, Y., Takami, N., Mori, M. X., Honda, A., and Inoue, R. (2008) *J. Physiol.* **586,** 4209–4223
29. Takimoto, E., Champion, H. C., Li, M., Belardi, D., Ren, S., Rodriguez, E. R., Bedja, D., Gabrielson, K. L., Wang, Y., and Kass, D. A. (2005) *Nat. Med.* **11,** 214–222
30. Hsu, S., Nagayama, T., Koitabashi, N., Zhang, M., Zhou, L., Bedja, D., Gabrielson, K. L., Molkentin, J. D., Kass, D. A., and Takimoto, E. (2009) *Cardiovasc. Res.* **81,** 301–309
31. Lewis, G. D., Lachmann, J., Camuso, J., Lepore, J. J., Shin, J., Martinovic, M. E., Systrom, D. M., Bloch, K. D., and Semigran, M. J. (2007) *Circulation* **115,** 59–66
32. Takimoto, E., Koitabashi, N., Hsu, S., Ketner, E. A., Zhang, M., Nagayama, T., Bedja, D., Gabrielson, K. L., Blanton, R., Siderovski, D. P., Mendelsohn, M. E., and Kass, D. A. (2009) *J. Clin. Invest.* **119,** 408–420
33. Nishida, M., Maruyama, Y., Tanaka, R., Kontani, K., Nagao, T., and Kurose, H. (2000) *Nature* **408,** 492–495
34. Nishida, M., Onohara, N., Sato, Y., Suda, R., Ogushi, M., Tanabe, S., Inoue, R., Mori, Y., and Kurose, H. (2007) *J. Biol. Chem.* **282,** 23117–23128
35. Nishida, M., Sugimoto, K., Hara, Y., Mori, E., Morii, T., Kurosaki, T., and Mori, Y. (2003) *EMBO J.* **22,** 4677–4688
36. Nishida, M., Tanabe, S., Maruyama, Y., Mangmool, S., Urayama, K., Nagamatsu, Y., Takagahara, S., Turner, J. H., Kozasa, T., Kobayashi, H., Sato, Y., Kawanishi, T., Inoue, R., Nagao, T., and Kurose, H. (2005) *J. Biol. Chem.* **280,** 18434–18441
37. Nishida, M., Sato, Y., Uemura, A., Narita, Y., Tozaki-Saitoh, H., Nakaya, M., Ide, T., Suzuki, K., Inoue, K., Nagao, T., and Kurose, H. (2008) *EMBO J.* **27,** 3104–3115
38. Higazi, D. R., Fearnley, C. J., Drawnel, F. M., Talasila, A., Corps, E. M., Ritter, O., McDonald, F., Mikoshiba, K., Bootman, M. D., and Roderick, H. L. (2009) *Mol. Cell* **33,** 472–482
39. Dietrich, A., Mederos y Schnitzler, M., Emmel, J., Kalwa, H., Hofmann, T., and Gudermann, T. (2003) *J. Biol. Chem.* **278,** 47842–47852
40. Huang, J., Zhou, H., Mahavadi, S., Sriwai, W., and Murthy, K. S. (2007) *Am. J. Physiol. Cell Physiol.* **292,** C200–C208
41. Tokudome, T., Kishimoto, I., Horio, T., Arai, Y., Schwenke, D. O., Hino, J., Okano, I., Kawano, Y., Kohno, M., Miyazato, M., Nakao, K., and Kangawa, K. (2008) *Circulation* **117,** 2329–2339
42. Mederos y Schnitzler, M., Storch, U., Meibers, S., Nurwakagari, P., Breit, A., Essin, K., Gollasch, M., and Gudermann, T. (2008) *EMBO J.* **27,** 3092–3103
43. Inoue, R., Jensen, L. J., Jian, Z., Shi, J., Hai, L., Lurie, A. I., Henriksen, F. H., Salomonsson, M., Morita, H., Kawarabayashi, Y., Mori, M., Mori, Y., and Ito, Y. (2009) *Circ. Res.* **104,** 1399–1409
44. Gottlieb, P., Folgering, J., Maroto, R., Raso, A., Wood, T. G., Kurosky, A., Bowman, C., Bichet, D., Patel, A., Sachs, F., Martinac, B., Hamill, O. P., Honoré, E. (2008) *Pflugers Arch.* **455,** 1097–1103
45. Dietrich, A., Mederos Y Schnitzler, M., Gollasch, M., Gross, V., Storch, U., Dubrovska, G., Obst, M., Yildirim, E., Salanova, B., Kalwa, H., Essin, K., Pinkenburg, O., Luft, F. C., Gudermann, T., and Birnbaumer, L. (2005) *Mol. Cell. Biol.* **25,** 6980–6989
46. Trebak, M., Vazquez, G., Bird, G. S., and Putney, J. W., Jr. (2003) *Cell Calcium* **33,** 451–461